Karolchik, D., Bruen, T. C., Bevan, R., Cutler, D. J., Schwartz, S., Elnitski, L., Idol, J. R., Prasad, A. B., Lee-Lin, S. Q., Maduro, V. V., Summers, T. J., Portnoy, M. E., Dietrich, N. L., Akhter, N., Ayele, K., Benjamin, B., Cariaga, K., Brinkley, C. P., Brooks, S. Y., Granite, S., Guan, X., Gupta, J., Haghighi, P., Ho, S. L., Huang, M. C., Karlins, E., Laric, P. L., Legaspi, R., Lim, M. J., Maduro, Q. L., Masiello, C. A., Mastrian, S. D., McCloskey, J. C., Pearson, R., Stantripop, S., Tiongson, E. E., Tran, J. T., Tsurgeon, C., Vogt, J. L., Walker, M. A., Wetherby, K. D., Wiggins, L. S., Young, A. C., Zhang, L. H., Osoegawa, K., Zhu, B., Zhao, B., Shu, C. L., De Jong, P. J., Lawrence, C. E., Smit, A. F., Chakravarti, A., Haussler, D., Green, P., Miller, W., and Green, E. D. (2003) Comparative analyses of multi-species sequences from targeted genomic regions. *Nature* **424,** 788–793

27. Woolfe, A., Goodson, M., Goode, D. K., Snell, P., McEwen, G. K., Vavouri, T., Smith, S. F., North, P., Callaway, H., Kelly, K., Walter, K., Abnizova, I., Gilks, W., Edwards, Y. J., Cooke, J. E., and Elgar, G. (2005) Highly conserved non-coding sequences are associated with vertebrate development. *PLoS Biol.* **3,** e7
28. Bell, A. C., West, A. G., and Felsenfeld, G. (1999) The protein CTCF is required for the enhancer blocking activity of vertebrate insulators. *Cell* **98,** 387–396
29. Felsenfeld, G., Burgess-Beusse, B., Farrell, C., Gaszner, M., Ghirlando, R., Huang, S., Jin, C., Litt, M., Magdinier, F., Mutskov, V., Nakatani, Y., Tagami, H., West, A., and Yusufzai, T. (2004) Chromatin boundaries and chromatin domains. *Cold Spring Harb. Symp. Quant. Biol.* **69,** 245–250
30. Shen, Y., Yue, F., McCleary, D. F., Ye, Z., Edsall, L., Kuan, S., Wagner, U., Dixon, J., Lee, L., Lobanenkov, V. V., and Ren, B. (2012) A map of the cis-regulatory sequences in the mouse genome. *Nature* **488,** 116–120
31. Birney, E., Stamatoyannopoulos, J. A., Dutta, A., Guigo, R., Gingeras, T. R., Margulies, E. H., Weng, Z., Snyder, M., Dermitzakis, E. T., Thurman, R. E., Kuehn, M. S., Taylor, C. M., Neph, S., Koch, C. M., Asthana, S., Malhotra, A., Adzhubei, I., Greenbaum, J. A., Andrews, R. M., Flicek, P., Boyle, P. J., Cao, H., Carter, N. P., Clelland, G. K., Davis, S., Day, N., Dhami, P., Dillon, S. C., Dorschner, M. O., Fiegler, H., Giresi, P. G., Goldy, J., Hawrylycz, M., Haydock, A., Humbert, R., James, K. D., Johnson, B. E., Johnson, E. M., Frum, T. T., Rosenzweig, E. R., Karnani, N., Lee, K., Lefebvre, G. C., Navas, P. A., Neri, F., Parker, S. C., Sabo, P. J., Sandstrom, R., Shafer, A., Vetrie, D., Weaver, M., Wilcox, S., Yu, M., Collins, F. S., Dekker, J., Lieb, J. D., Tullius, T. D., Crawford, G. E., Sunyaev, S., Noble, W. S., Dunham, I., Denoeud, F., Reymond, A., Kapranov, P., Rozowsky, J., Zheng, D., Castelo, R., Frankish, A., Harrow, J., Ghosh, S., Sandelin, A., Hofacker, I. L., Baertsch, R., Keefe, D., Dike, S., Cheng, J., Hirsch, H. A., Sekinger, E. A., Lagarde, J., Abril, J. F., Shahab, A., Flamm, C., Fried, C., Hackermuller, J., Hertel, J., Lindemeyer, M., Missal, K., Tanzer, A., Washietl, S., Korbel, J., Emanuelsson, O., Pedersen, J. S., Holroyd, N., Taylor, R., Swarbreck, D., Matthews, N., Dickson, M. C., Thomas, D. J., Weirauch, M. T., Gilbert, J., Drenkow, J., Bell, I., Zhao, X., Srinivasan, K. G., Sung, W. K., Ooi, H. S., Chiu, K. P., Foissac, S., Alioto, T., Brent, M., Pachter, L., Tress, M. L., Valencia, A., Choo, S. W., Choo, C. Y., Ucla, C., Manzano, C., Wyss, C., Cheung, E., Clark, T. G., Brown, J. B., Ganesh, M., Patel, S., Tammana, H., Chrast, J., Henrichsen, C. N., Kai, C., Kawai, J., Nagalakshmi, U., Wu, J., Lian, Z., Lian, J., Newburger, P., Zhang, X., Bickel, P., Mattick, J. S., Carninci, P., Hayashizaki, Y., Weissman, S., Hubbard, T., Myers, R. M., Rogers, J., Stadler, P. F., Lowe, T. M., Wei, C. L., Ruan, Y., Struhl, K., Gerstein, M., Antonarakis, S. E., Fu, Y., Green, E. D., Karaoz, U., Siepel, A., Taylor, J., Liefer, L. A., Wetterstrand, K. A., Good, P. J., Feingold, E. A., Guyer, M. S., Cooper, G. M., Asimenos, G., Dewey, C. N., Hou, M., Nikolaev, S., Montoya-Burgos, J. I., Loytynoja, A., Whelan, S., Pardi, F., Massingham, T., Huang, H., Zhang, N. R., Holmes, I., Mullikin, J. C., Ureta-Vidal, A., Paten, B., Seringhaus, M., Church, D., Rosenbloom, K., Kent, W. J., Stone, E. A., Batzoglou, S., Goldman, N., Hardison, R. C., Haussler, D., Miller, W., Sidow, A., Trinklein, N. D., Zhang, Z. D., Barrera, L., Stuart, R., King, D. C., Ameur, A., Enroth, S., Bieda, M. C., Kim, J., Bhinge, A. A., Jiang, N., Liu, J., Yao, F., Vega, V. B., Lee, C. W., Ng, P., Shahab, A., Yang, A., Moqtaderi, Z., Zhu, Z., Xu, X., Squazzo, S., Oberley, M. J., Inman, D., Singer, M. A., Richmond, T. A., Munn, K. J., Rada-Iglesias, A., Wallerman, O., Komorowski, J., Fowler, J. C., Couttet, P., Bruce, A. W., Dovey, O. M., Ellis, P. D., Langford, C. F., Nix, D. A., Euskirchen, G., Hartman, S., Urban, A. E., Kraus, P., Van Calcar, S., Heintzman, N., Kim, T. H., Wang, K., Qu, C., Hon, G., Luna, R., Glass, C. K., Rosenfeld, M. G., Aldred, S. F., Cooper, S. J., Halees, A., Lin, J. M., Shulha, H. P., Zhang, X., Xu, M., Haidar, J. N., Yu, Y., Ruan, Y., Iyer, V. R., Green, R. D., Wadelius, C., Farnham, P. J., Ren, B., Harte, R. A., Hinrichs, A. S., Trumbower, H., Clawson, H., Hillman-Jackson, J., Zweig, A. S., Smith, K., Thakkapallayil, A., Barber, G., Kuhn, R. M., Karolchik, D., Armengol, L., Bird, C. P., de Bakker, P. I., Kern, A. D., Lopez-Bigas, N., Martin, J. D., Stranger, B. E., Woodroffe, A., Davydov, E., Dimas, A., Eyras, E., Hallgrimsdottir, I. B., Huppert, J., Zody, M. C., Abecasis, G. R., Estivill, X., Bouffard, G. G., Guan, X., Hansen, N. F., Idol, J. R., Maduro, V. V., Maskeri, B., McDowell, J. C., Park, M., Thomas, P. J., Young, A. C., Blakesley, R. W., Muzny, D. M., Sodergren, E., Wheeler, D. A., Worley, K. C., Jiang, H., Weinstock, G. M., Gibbs, R. A., Graves, T., Fulton, R., Mardis, E. R., Wilson, R. K., Clamp, M., Cuff, J., Gnerre, S., Jaffe, D. B., Chang, J. L., Lindblad-Toh, K., Lander, E. S., Koriabine, M., Nefedov, M., Osoegawa, K., Yoshinaga, Y., Zhu, B., and de Jong, P. J. (2007) Identification and analysis of functional elements in 1% of the human genome by the ENCODE pilot project. *Nature* **447,** 799–816
32. Blow, M. J., McCulley, D. J., Li, Z., Zhang, T., Akiyama, J. A., Holt, A., Plajzer-Frick, I., Shoukry, M., Wright, C., Chen, F., Afzal, V., Bristow, J., Ren, B., Black, B. L., Rubin, E. M., Visel, A., and Pennacchio, L. A. (2010) ChIP-Seq identification of weakly conserved heart enhancers. *Nat. Genet.* **42,** 806–810
33. Koch, F., Jourquin, F., Ferrier, P., and Andrau, J. C. (2008) Genome-wide RNA polymerase II: not genes only!. *Trends Biochem. Sci.* **33,** 265–273
34. Szutorisz, H., Dillon, N., and Tora, L. (2005) The role of enhancers as centres for general transcription factor recruitment. *Trends Biochem. Sci.* **30,** 593–599
35. Sei, C. A., Irons, C. E., Sprenkle, A. B., McDonough, P. M., Brown, J. H., and Glembotski, C. C. (1991) The α-adrenergic stimulation of atrial natriuretic factor expression in cardiac myocytes requires calcium influx, protein kinase C, and calmodulin-regulated pathways. *J. Biol. Chem.* **266,** 15910–15916
36. Iaccarino, G., Dolber, P. C., Lefkowitz, R. J., and Koch, W. J. (1999) Bβ-adrenergic receptor kinase-1 levels in catecholamine-induced myocardial hypertrophy: regulation by beta- but not alpha1-adrenergic stimulation. *Hypertension* **33,** 396–401
37. Seidman, C. E., Wong, D. W., Jarcho, J. A., Bloch, K. D., and Seidman, J. G. (1988) *Cis*-acting sequences that modulate atrial natriuretic factor gene expression. *Proc. Natl. Acad. Sci. U. S. A.* **85,** 4104–4108
38. Thuerauf, D. J., and Glembotski, C. C. (1997) Differential effects of protein kinase C, Ras, and Raf-1 kinase on the induction of the cardiac B-type natriuretic peptide gene through a critical promoter-proximal M-CAT element. *J. Biol. Chem.* **272,** 7464–7472

Received for publication November 12, 2013.
Accepted for publication January 2, 2014.

Cardiovascular Research (2014) **102**, 6–8
doi:10.1093/cvr/cvu051

EDITORIAL

Dickkopf-3: a stubborn protector of cardiac hypertrophy

Hiroshi Akazawa[1,2,3] and Issei Komuro[2,3,4]*

[1]Department of Advanced Clinical Science and Therapeutics, Graduate School of Medicine, The University of Tokyo, Tokyo, Japan; [2]Department of Cardiovascular Medicine, Graduate School of Medicine, The University of Tokyo, Tokyo, Japan; [3]CREST, Japan Science and Technology Agency, Chiyoda-ku, Tokyo, Japan; and [4]Institute for Academic Initiatives, Osaka University, Suita, Osaka, Japan

Online publish-ahead-of-print 3 March 2014

This editorial refers to 'Dickkopf-3 attenuates pressure overload-induced cardiac remodelling' by Y. Zhang *et al.*, pp. 35–45, this issue.

In response to haemodynamic overload under pathological conditions such as hypertension, valvular heart disease, and myocardial infarction, the heart undergoes hypertrophic growth by increasing cell size and protein synthesis as well as changing the transcriptional programme in cardiac myocytes.[1] Although cardiac hypertrophy is beneficial in the way that it reduces ventricular wall tension and maintains pump function, it promotes cardiac structural remodelling and dysfunction, and eventually leads to development of congestive heart failure, arrhythmia, and sudden death. At present, several drugs such as inhibitors of the renin–angiotensin–aldosterone system, β-adrenergic receptor blockers, and calcium channel blockers are clinically available for the management of hypertension, and these drugs have shown significant efficacy in preventing load-induced cardiac hypertrophy and remodelling. However, these pharmacological agents are currently of limited effectiveness, and further discovery and development of novel classes of cardioprotective drugs are in urgent need.[2] For that purpose, it is important to elucidate the molecular mechanisms underlying the development of cardiac hypertrophy. In the article by Zhang *et al.*,[3] integrating genetic approaches in mice have shed light on Dickkopf-3 (DKK3) as a cardioprotective regulator of cardiac hypertrophy.

DKK3 is a secreted glycoprotein of the Dickkopf family that typically antagonizes the Wnt/β-catenin signalling by interfering with Wnt co-receptors, low-density lipoprotein receptor-related protein and kremen.[4] 'Dickkopf' is a German word for 'big head' or 'stubborn', and the protein family owes its name to the finding that DKK1 is sufficient and necessary to induce head formation in *Xenopus* embryo.[5] Zhang *et al.*[3] first demonstrated that cardiac expression of DKK3 was downregulated in patients with end-stage heart failure and in mice with pressure-overloaded cardiac hypertrophy. In neonatal rat cardiac myocyte cultures, angiotensin II-induced hypertrophic responses were enhanced by siRNA-mediated knockdown of DKK3, and conversely were attenuated by overexpression of DKK3. Consistently, cardiac hypertrophy following aortic banding in mice was enhanced by genetic disruption of DKK3, and was attenuated by transgenic overexpression of DKK3. These loss- and gain-of-function analyses, both *in vitro* and *in vivo*, indicated the regulatory role of DKK3 in protecting the heart from the development of pathological cardiac hypertrophy. The next obvious question is how DKK3 affects the signalling effectors underlying pathological hypertrophy and remodelling of the heart. Zhang *et al.* demonstrated that DKK3 inhibited the activation of apoptosis signal-regulating kinase 1 (ASK1), and thereby suppressed the activation of its downstream effectors c-Jun N-terminal kinases (JNKs) and p38 mitogen-activated protein kinases (MAPKs) in hearts subjected to hypertrophic stimulation (*Figure 1*). Importantly, DKK3 overexpression attenuated the activation of ASK1 in pressure-overloaded hearts of mice, and restoration of ASK1 activity by transgenic overexpression abolished the protective effects of DKK3 overexpression against pressure overload-induced cardiac remodelling. Conversely, disruption of DKK3 enhanced the ASK1 activation in pressure-overloaded hearts, and inactivation of ASK1 by transgenic overexpression of a dominant negative mutant prevented exaggeration of pressure overload-induced cardiac remodelling in DKK3-deficient mice.

ASK1 is a key component of a high molecular mass complex, termed the ASK1 signalosome, and is activated in response to a variety of cellular stresses, such as reactive oxygen species (ROS), endoplasmic reticulum (ER) stress, calcium overload, and inflammatory signals mediated by tumour necrosis factor-α (TNF-α) and lipopolysaccharide.[6] While the ASK1 activity is suppressed by the reduced form of thioredoxin (Trx) (a redox-sensitive protein) within the ASK1 signalosome, oxidation of Trx in response to ROS induced autophosphorylation and oligomerization of ASK1, leading to its activation. Upon ROS-stimulated activation, adaptor proteins, such as TNF-α receptor-associated factor 2 (TRAF2) and TRAF6, and USP9X deubiquitination enzyme are recruited to the signalosome to maintain full activation of ASK1[6] (*Figure 1*). Although the precise mechanism by which DKK3 inhibits ASK1 activation remains unclear, Zhang *et al.*[3] demonstrated, by co-immunoprecipitation experiments, that exogenously expressed DKK3 and ASK1 formed a complex in HEK293 T cells, and furthermore showed direct interaction between endogenous DKK3 and ASK1 in neonatal rat cardiac myocytes. These results suggest that DKK3 may interfere with ASK1 activation via the physical interaction with ASK1 within the signalosome (*Figure 1*), but

* Corresponding author. Tel: +81 338155411; fax: +81 338152087, Email: komuro-tky@umin.ac.jp

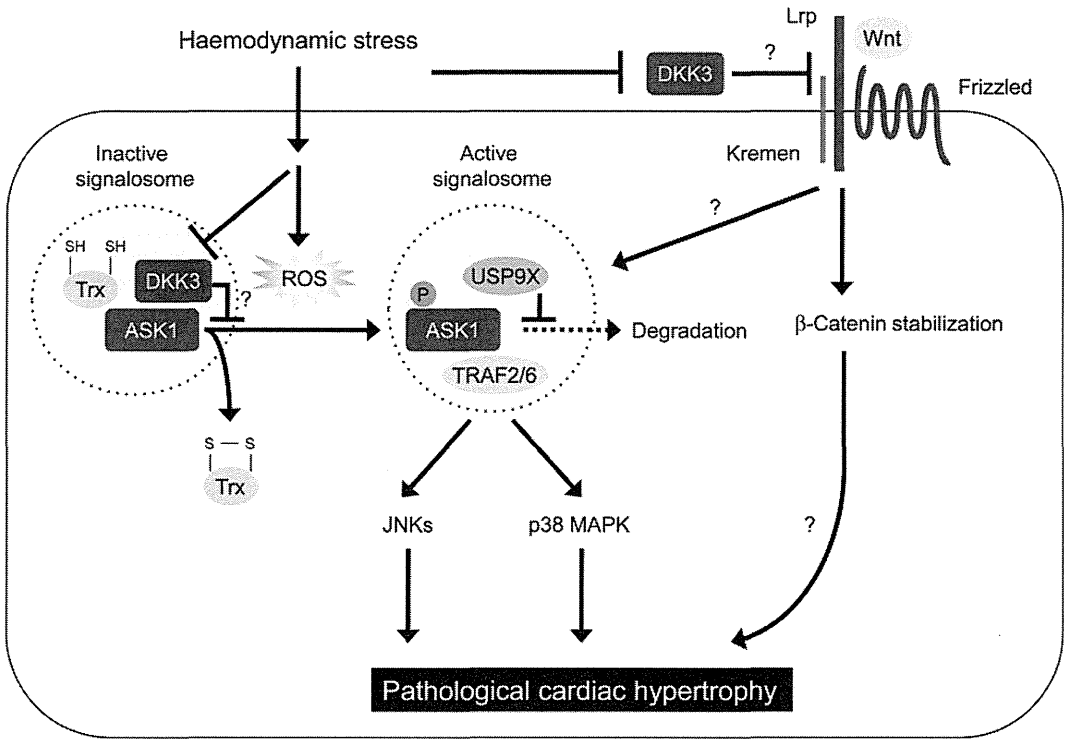

Figure 1 DKK3-induced cardioprotection against pathological cardiac hypertrophy. ASK1 activity is suppressed by the reduced form of Trx within the ASK1 signalosome, but ROS-induced oxidation of Trx induced phosphorylation and activation of ASK1 in haemodynamically stressed hearts. In the active signalosome, adaptor proteins such as TRAF2 and TRAF6, and USP9X deubiquitination enzyme are recruited to maintain full activation of ASK1. Fully activated ASK1 promotes pathological cardiac hypertrophy via the JNKs and p38 MAPK pathways. DKK3 is down-regulated in stressed hearts, and restoration of DKK3 attenuated activation of the ASK1-JNKs/p38 MAPK pathways, leading to the prevention of pathological cardiac hypertrophy in mice. DKK3 forms a complex with ASK1, and may interfere the process of ASK1 activation through the physical interaction within the signalosome.

clearly leave many open questions: which domains of these two proteins are responsible for mutual binding? How does DKK3 influence the composition of proteins within the ASK1 signalosome in the presence or absence of ROS? As mentioned above, DKK3 is a secreted protein, and possesses an N-terminal signal sequence.[4] Recent studies have shown intracellular localization of DKK3,[7–9] and such localization can be explained by the fact that the signal sequence is readily recognized by the signal recognition particle that catalyses the transport of the secretory precursor protein into the ER lumen.[10] Indeed, immunofluorescence staining indicated localization of DKK3 at perinuclear structures such as ER and Golgi apparatus,[8,9,11] but direct interactions between DKK3 and cytosolic proteins such as βTrCP[12] and dynein light chain Tctex-1 were also reported.[11] Although Zhang *et al.*[3] showed an intracellular distribution of DKK3 by immunohistochemical analysis of human hearts, further studies are necessary to determine where and how DKK3 forms a complex with the cytosolic protein kinase ASK1 in cardiac myocytes.

It also remains unsolved whether antagonization of the Wnt/β-catenin signalling is involved in the cardioprotection by DKK3 against hypertrophic stimulation. Although there have been conflicting data on the effects of β-catenin stabilization on pathological hypertrophy in mice,[13] Noh *et al.*[14] recently reported that Wnt-3a negatively regulates the protein level and kinase activity of ASK1 by inhibiting glycogen synthase kinase-3β in murine L929 fibrosarcoma cells. Since the ability of DKK3 to inhibit the Wnt/β-catenin signalling appears to be context dependent, it is of interest to investigate the impact of loss- and gain-of-function of DKK3 on the Wnt/β-catenin signalling in cardiac myocytes under stressed conditions.

Accumulating evidence has indicated that DKK3 is down-regulated in human cancer cells, and DKK3 emerges as a potential tumour biomarker and a promising molecular target for cancer therapy.[15] The study of Zhang *et al.*[3] provides an initial but important clue towards a new strategy to modulate the DKK3 function for treatment of heart diseases. Of course, further studies are required to explore more precise mechanism of DKK3-mediated cardioprotection and to develop an optimal way to restore the expression and function of DKK3 in stressed hearts.

Conflict of interest: none declared.

Funding

This work was supported in part by grants from Japan Society for the Promotion of Science (KAKENHI 21229010, 23390213, 24659390) and Health and Labor Sciences Research Grants.

References

1. Akazawa H, Komuro I. Roles of cardiac transcription factors in cardiac hypertrophy. *Circ Res* 2003;**92**:1079–1088.
2. Landmesser U, Drexler H. Chronic heart failure: an overview of conventional treatment versus novel approaches. *Nat Clin Pract Cardiovasc Med* 2005;**2**:628–638.
3. Zhang Y, Liu Y, Zhu X, Zhang X, Jiang D, Bian Z, Zhang X, Chen K, Wei X, Gao L, Zhu L, Yang Q, Fan G, Lau W, Ma X, Li H. Dickkopf-3 attenuates pressure overload-induced cardiac remodeling. *Cardiovasc Res* 2014;**102**:35–45.

4. Niehrs C. Function and biological roles of the Dickkopf family of Wnt modulators. *Oncogene* 2006;**25**:7469–7481.
5. Glinka A, Wu W, Delius H, Monaghan AP, Blumenstock C, Niehrs C. Dickkopf-1 is a member of a new family of secreted proteins and functions in head induction. *Nature* 1998;**391**:357–362.
6. Takeda K, Noguchi T, Naguro I, Ichijo H. Apoptosis signal-regulating kinase 1 in stress and immune response. *Annu Rev Pharmacol Toxicol* 2008;**48**:199–225.
7. Hsieh SY, Hsieh PS, Chiu CT, Chen WY. Dickkopf-3/REIC functions as a suppressor gene of tumor growth. *Oncogene* 2004;**23**:9183–9189.
8. Nakamura RE, Hackam AS. Analysis of Dickkopf3 interactions with Wnt signaling receptors. *Growth Factors* 2010;**28**:232–242.
9. Zhang K, Watanabe M, Kashiwakura Y, Li SA, Edamura K, Huang P, Yamaguchi K, Nasu Y, Kobayashi Y, Sakaguchi M, Ochiai K, Yamada H, Takei K, Ueki H, Huh NH, Li M, Kaku H, Na Y, Kumon H. Expression pattern of REIC/Dkk-3 in various cell types and the implications of the soluble form in prostatic acinar development. *Int J Oncol* 2010;**37**:1495–1501.
10. Akopian D, Shen K, Zhang X, Shan SO. Signal recognition particle: an essential protein-targeting machine. *Annu Rev Biochem* 2013;**82**:693–721.
11. Ochiai K, Watanabe M, Ueki H, Huang P, Fujii Y, Nasu Y, Noguchi H, Hirata T, Sakaguchi M, Huh NH, Kashiwakura Y, Kaku H, Kumon H. Tumor suppressor REIC/Dkk-3 interacts with the dynein light chain, Tctex-1. *Biochem Biophys Res Commun* 2011;**412**:391–395.
12. Lee EJ, Jo M, Rho SB, Park K, Yoo YN, Park J, Chae M, Zhang W, Lee JH. Dkk3, downregulated in cervical cancer, functions as a negative regulator of beta-catenin. *Int J Cancer* 2009;**124**:287–297.
13. Naito AT, Shiojima I, Komuro I. Wnt signaling and aging-related heart disorders. *Circ Res* 2010;**107**:1295–1303.
14. Noh KT, Park YM, Cho SG, Choi EJ. GSK-3beta-induced ASK1 stabilization is crucial in LPS-induced endotoxin shock. *Exp Cell Res* 2011;**317**:1663–1668.
15. Veeck J, Dahl E. Targeting the Wnt pathway in cancer: the emerging role of Dickkopf-3. *Biochim Biophys Acta* 2012;**1825**:18–28.

OPEN ACCESS Freely available online

PLOS | ONE

Src Is Required for Mechanical Stretch-Induced Cardiomyocyte Hypertrophy through Angiotensin II Type 1 Receptor-Dependent β-Arrestin2 Pathways

Shijun Wang[1,2☯], Hui Gong[1,2☯], Guoliang Jiang[2☯], Yong Ye[2☯], Jian Wu[2], Jieyun You[2], Guoping Zhang[2], Aijun Sun[1,2], Issei Komuro[3], Junbo Ge[1,2], Yunzeng Zou[1,2]*

1 Shanghai Institute of Cardiovascular Diseases, Zhongshan Hospital, Fudan University, Shanghai, China, **2** Institutes of Biomedical Science, Fudan University, Shanghai, China, **3** Department of Cardiovascular Medicine, the University of Tokyo Graduate School of Medicine, Tokyo, Japan

Abstract

Angiotensin II (AngII) type 1 receptor (AT1-R) can be activated by mechanical stress (MS) without the involvement of AngII during the development of cardiomyocyte hypertrophy, in which G protein-independent pathways are critically involved. Although β-arrestin2-biased signaling has been speculated, little is known about how AT1-R/β-arrestin2 leads to ERK1/2 activation. Here, we present a novel mechanism by which Src kinase mediates AT1-R/β-arrestin2-dependent ERK1/2 phosphorylation in response to MS. Differing from stimulation by AngII, MS-triggered ERK1/2 phosphorylation is neither suppressed by overexpression of RGS4 (the negative regulator of the G-protein coupling signal) nor by inhibition of Gαq downstream protein kinase C (PKC) with GF109203X. The release of inositol 1,4,5-triphosphate (IP_3) is increased by AngII but not by MS. These results collectively suggest that MS-induced ERK1/2 activation through AT1-R might be independent of G-protein coupling. Moreover, either knockdown of β-arrestin2 or overexpression of a dominant negative mutant of β-arrestin2 prevents MS-induced activation of ERK1/2. We further identifies a relationship between Src, a non-receptor tyrosine kinase and β-arrestin2 using analyses of co-immunoprecipitation and immunofluorescence after MS stimulation. Furthermore, MS-, but not AngII-induced ERK1/2 phosphorylation is attenuated by Src inhibition, which also significantly improves pressure overload-induced cardiac hypertrophy and dysfunction in mice lacking AngII. Finally, MS-induced Src activation and hypertrophic response are abolished by candesartan but not by valsartan whereas AngII-induced responses can be abrogated by both blockers. Our results suggest that Src plays a critical role in MS-induced cardiomyocyte hypertrophy through β-arrestin2-associated angiotensin II type 1 receptor signaling.

Citation: Wang S, Gong H, Jiang G, Ye Y, Wu J, et al. (2014) Src Is Required for Mechanical Stretch-Induced Cardiomyocyte Hypertrophy through Angiotensin II Type 1 Receptor-Dependent β-Arrestin2 Pathways. PLoS ONE 9(4): e92926. doi:10.1371/journal.pone.0092926

Editor: Tianqing Peng, University of Western Ontario, Canada

Received January 25, 2014; **Accepted** February 26, 2014; **Published** April 3, 2014

Funding: This work was supported by the National Natural Science Fund of China (81220108003; 81000041); China Doctoral Foundation (20110071110051) and Technology Commission of Shanghai Municipality (11JC1402400). The funders had no role in study design, data collection and analysis, decision to publish, or preparation of the manuscript.

Competing Interests: The authors have declared that no competing interests exist.

* E-mail: zou.yunzeng@zs-hospital.sh.cn

☯ These authors contributed equally to this work.

Introduction

Angiotensin II type 1 (AT1) receptor, belonging to the G-protein-coupled receptor family (GPCRs), shares a common structure of 7-transmembrane receptor (7TMRs), and mediates the signal response of Angiotensin II (AngII), thereby regulates blood pressure, cardiac hypertrophy and heart failure [1,2]. Recent studies demonstrate that AT1-R acts as a stress-sensitive switcher which can be triggered by mechanical stress without the ligand binding [3–5]. We have previously showed that some kinds of angiotensin II receptor blockers (ARBs), such as candesartan and olmesartan, inhibit pressure overload-induced cardiac hypertrophy in angiotensinogen knockout (AGT KO) mice, while others like valsartan, exert the inhibitory effect in the presence of AngII [6]. However, the detailed molecular mechanisms of how mechanical stress-induced AT1-R activation and its inhibition are regulated by ARBs still remain elucidative.

A growing body of evidences indicated that biased agonism might selectively induce the conformational switch of GPCRs, which preferentially activated or inhibited a subset of downstream signaling [7,8]. We thus assumed there might be an unique pathway involved in mechanical stress (MS)-induced AT1-R activation and signal transduction, which was different from that induced by AngII, and resulted in the divergent effects of various ARBs. Rakesh K. previously reported that β-arrestin2 dependent pathway rather than G-protein coupling played a pivotal role in MS-induced AT1-R signaling [7]. However, little was known regarding to the downstream pathway subsequent to β-arrestin2-mediated AT1-R and ERK1/2 activation by mechanical stress. It was believed that AngII stimulated G-protein-dependent ERK1/2 activation through binding to AT1-R, but overexpression of AT1-R mutant lacking Gαq/Gαi coupling also induced ERK1/2 phosphorylation and developed severe myocardial hypertrophy both in vitro and in vivo [9,10]. We previously reported that G protein-independent calcineurin was critically involved in me-

chanical stretch induced myocardial hypertrophy [11], and candesartan could attenuate the hypertrophic response through regulating the tyrosine kinases cascade [3]. Therefore, we hypothesized that Src family kinase, the non-receptor tyrosine kinase, might mediate G protein-independent AT1-R signaling and cardiac hypertrophy induced by MS.

Src is a stress-sensitive kinase which plays an important role in the pathophysiological mechanisms for pressure overload-induced myocardial hypertrophy and pulmonary arterial hypertension, Src inhibition can effectively reverse the hypertensive response and hypertrophic signaling [12,13]. MS-mediated autophosphorylation of Src is highly associated with ERK1/2 activation [14]. Recent study revealed the expression and distribution of Src in the nucleus of cardiomyocytes with hypertrophy [15], and β-arrestin2 enhanced nuclear localization of ERK1/2 via GPCRs activation [16]. Mutant AT1 receptor lacking the docking site impaired Src-dependent nuclear translocation of ERK1/2 [10]. These findings prompted us to assume that Src kinase might be involved in β-arrestin2-meidated ERK1/2 activation and cardiac hypertrophy subsequent to AT1-R activation by MS. In the present study, we focused on the changes of AT1-R downstream signals, especially the role of Src kinase, in regulating β-arrestin2-dependent and AT1-R-induced signal transduction after MS.

Materials and Methods

Reagents

Anti-ERK1/2 (#9102), anti-phospho-ERK1/2 at Thr^{202}/Tyr^{204} (#9101) and anti-phospho-Src at Tyr^{416} (#2101) were purchased from Cell-signaling Technology; anti-Angiotensin II type 1 receptor (ab9391) were purchased from Abcam, plc; anti-FLAG-probe (#F7425), GF109203X (#G2911) were purchased from Sigma-Aldrich; anti-HA-probe (sc-805), anti-β-arrestin2 (sc-13140) were purchased from Santa Cruz Biotechnology; and SU6656 (#572635) was purchased from Calbiochem, Merck KGaA. Mechanic stretch-model culture plates were provided as kind gifts from Chiba University Graduate School of Medicine.

Plasmids Constructs

HA-tagged ERK2, FLAG-tagged β-arrestin1 and 2 were kindly provided by professor Issei Komuro (Tokyo University, Japan). Wild-type FLAG-tagged β-arrestin2 in vector pcDNA3 was used as the template. PCR based site-directed mutagenesis approach was performed to make a valine(54)-to-aspartic substitution in the wild-type β-arrestin2 using Pfu polymerase (Takara), the mutagenic primers were as follows: 5′-GACCGGAAAGACTTTGTGACC-3′ (forward) and 5′-GGTCACAAAGTCTTTCCGGTC-3′ (reverse). The mutant β-arrestin2-V54D was amplified and then cloned into plasmid pcDNA3. The SRC gene was amplified by PCR using primers 5′-CGGGATCCACTAGTAACGGCCGCCAG-3′ (forward) with a *BamH*I restriction site and 5′-CGCTCGAGCGAGGTTCTCTCCAGGCTG-3′ with a *Xho*I restriction site, and subcloned into the pcDNA3 plasmid containing a HA tag-encoding sequence.

Cell Culture and transfection

In vitro cardiacmyocytes were cultured as previously reported [34]. In brief, neonatal (one-day-old) rats were sacrificed under ether anesthesia, and then ventricular tissues were surgically isolated from the anesthetized rats, all operations were made to minimize suffering. The isolated tissues were minced and placed in culture medium containing the buffers of 5.4 mmol/L KCl, 0.44 mmol/L NaH_2PO_4, 137 mmol/L NaCl, 4.2 mmol/L $NaHCO_3$ and 5 mmol/L glucose at pH 7.4. Cells were then dissociated at 37°C by a combination of mechanical agitation and enzymatic digestion with 0.1 mg/mL DNase II (Sigma) and 0.125% pancreatin trypsin (Calbiochem). Cells were pre-plated for 2 h in 100 mm dishes with Dulbecco's modified Eagle's medium (DMEM) with 10% defined bovine calf serum (FBS, HyClone), penicillin (100 units/mL) and streptomycin (100 mg/mL) (Sigma), then the unattached cardiomyocytes were collected and plated at a field density of 1×10^5 cells/cm^2 on silicone rubber culture dishes. Stretching of cardiacmyocytes by 10% was conducted as described previously [3]. HEK-293-AT1 cells lines were kindly provided by professor Issei Komuro (Tokyo University, Japan), and were cultured in Dulbecco's modified Eagles medium (DMEM) with 10% FBS and 1% penicillinystreptomycin as described previously [3]. Transient transfection of AT1 plasmids into cells were performed by using Gene Transfection System (Invitrogen) according to the manufacturer's instructions. The stable selection of transfection cells were achieved by adding Aminoglycoside G418 (200 ug/mL) to cells 3 day after transfection. All cell cultures were transferred to serum-free media 24 h before experiment.

Experimental Animal Model

Angiotensinogen gene knockout (AGT KO) mice were provided as kind gifts from professor Issei Komuro. Aged 8~10 weeks of AGT KO mice were used in the present study and wide-type (WT) C57BL/6 mice were used as control littermates. All the procedures involving animals were carried out in accordance with the recommendations of the guidelines for the Care and Use of Laboratory Animals from China Council on Animal Care. The experiment was approved by the Experimental Animal Ethics Committee, Fudan University Shanghai Medical College with the permit number of 20110307-092. Pressure overload model was established by transverse aorta constriction (TAC) for 2 weeks as previously described [6,11]. To ameliorate suffering, the mice were anesthetized by intraperitoneal injection of a combination of ketamine (100 mg/kg) with xylazine (5 mg/kg), and respiration was artificially controlled with a tidal volume of 0.2 ml and a respiratory rate of 110 breaths/min. The transverse aorta was constricted with the 7-0 nylon strings by ligating the aorta together with a blunted 27-gauge needle to yield a narrowing of 0.4 mm in diameter, and the needle was pulled out later. SU6656 (1 mg/kg/day) was continuously administered by Alzet osmotic mini pumps (DURECT, Cupertino, California) and was implanted subcutaneously into the back of mice right after anesthetized with 2% inhaled isoflurane from 3 days before TAC to 2 weeks after TAC. At 2 weeks after TAC, all mice were anesthetized by inhaled anesthetic isoflurane for cardiac echocardiography and hemodynamics analysis, and then mice were quickly sacrificed before they woke up. The hearts were excised for further examination, and the bodies were recorded, collected and centralized processing.

ERK2 kinase activity Assay

HA-tagged ERK2 plasmid was transient transfected into cardiomyocytes 24 h after plating the cells on stretch-model culture plates. ERK2 kinase activity was determined as we described previously [17]. In brief, RGS4 plasmid DNA (7.5 μg) was co-transfected into each dish of HEK-293-AT1 cells with or without HA tagged-ERK2 (2.5 μg), then the transfected cells were lysed, and the lysates were incubated with anti-HA antibody for 1 h at 4°C. Then, the immunocomplex was precipitated using A/G Plus-agarose beads, washed, resuspended in 25 ml kinase buffer with 2 m Ci of [γ-^{32}P] ATP, and incubated with 25 mg of MBP as the substrate at 25°C for 10 min. After incubation, the reaction was terminated by adding Laemmli sample buffer (0.002% bromphenol blue, 0.01M sodium phosphate buffer, pH 7.0, 10%

glycerol, 0.4%SDS, and 1% 2-mercaptoethanol) to the samples, and the samples were boiled for 5 min. The supernatants were subjected to SDS-polyacrylamide gel electrophoresis, and the gel was washed with 7% acetic acid for 30 min and with 3% glycerol for 30 min, dried, and then subjected to autoradiography.

RT-PCR analysis

Total RNA were extracted from cardiomyocytes using Trizol (Invitrogen) after mechanical stretch for 10 min. The cDNA was synthesized and optimized using a cDNA reverse transcription Kit (Takara), and the PCR primers used as follows:β-arrestin1, the sense primer:5′-CTGGATGTCTTGGGTCTGA-3′ and anti-sense primer: 3′-CGGATGGGGAAGTGGAAAC-5′; β-arrestin2, the sense primer: 5′-CCCTATGCTCAGAAACGAA-3′ and the anti-sense primer: 3′-TAGACAAGTAGCGGTGGAT-5′. The amplification of target genes were carried out on MJ Mini^{TM} Gradient Thermal Cycler with a program of 95°C for 3 min followed by 35 cycles of 95°C for 30 s, 54°C for 30 s and 72°C for 30 s, and by a single incubation at 72°C for 5 min. PCR products were separated by electrophoresis on 1.2% agarose gels.

Western blotting (WB) Analysis

Cardiomyocytes were digested and separated to mini tubes. After incubating with cell lysates for 30 min on ice, cells supernatant was obtained by centrifugating for 30 min.Total protein extracts were size-fractionated by SDS-PAGE and were transferred to PVDF membranes. The membranes were blocked with 5% FBS in TBS-T buffer (20 umol/L Tris pH 7.4, 150 mmol/L NaCl and 0.05% Tween 20) for 2 h, then were incubated with antibody at 4°C overnight. After washing them for 3 times, the second antibody was adding, finally the membranes were treated with supersignal West Pico Chemiluminescent Substrate (Thermo), and the immunoreactive bands were detected by chemiluminescence system (Bio-Rad).

Immunoprecipitation (IP) and WB analysis

Cultured cells were transfected with various plasmids as indicated. After transfection for 24 h, cells were harvested by lysis buffer (10 mmol/L Tris-HCl, pH 7.4, 150 mmol/L NaCl, 1 mmol/L EDTA, 1% Triton X-100, 2.5 mmol/L sodium pyrophosphate, 25 mmol/L β-glycerol phosphate, 10 mmol/L NaF, 10 μg/mL aprotinin, 10 μg/mL leupeptin, 1 mmol/L PMSF). Cell extracts were sonicated and then centrifuged at 15000 g for 30 min at 4°C. Supernatants were subjected to immunoprecipitaion with indicated antibodies and co-incubated with protein A/G Plus-agarose beads (Santa Cruz Biotechnology) at 4°C for 3 h. Then the beads were spun down at 800 g for 2 min, washed with 700 μL lysis buffer for 3 times. The beads were eluted with SDS/PAGE loading buffer after extensive washed with 0.1 mol/L Tris-buffered saline. Finally the immunoprecipitates and total cell lysates were subjected to SDS/PAGE and determined by Western blotting with indicated antibodies.

Immunocytochemistry Analysis

In vitro cultured cardiomyocytes were seeded in photic-bottomed stretch plate, and were transfected with β-arrestin2-GFP-WT or β-arrestin2-GFP-V54D mutant. Cells were stretched for 10 min, and washed with 1×PBS and fixed in 4% formaldehyde for 15 minutes at room temperature. After permeabililized with 0.1% triton X-100 for 10 minutes at room temperature, cells were blocked in 5% BSA for 1.5 hours. Immunostaining was performed by using anti-phospho-Src antibody overnight at 4°C. Oil immersion lens in a multitrack mode using a dual excitation (Alexa Fluor488 and Alexa Fluor555) filter sets. All Cells were counterstained with DAPI staining. Immunostaining was visualized by using laser scanning microscope (Leica Microsystems, Bensheim, Germany).

Detection of Inositol Phosphates

Determination of IP_3 was according to the methods as described previously [16]. In brief, cells were replated into 24-well plates at 1.5×10^5 cells per well and labeled for 24 h at 37°C with myo-[^{3}H] inositol (1.0 μCi/mL). After terminated labeling by aspirating the medium, cells were rinsing twice and the pellet was resuspended and harvested with phosphate-buffered saline (0.02% EDTA). Cells were transferred to culture template for re-adherence, and after subjecting to mechanical stretch or incubated with AngII (10^{-7} mol/L), cell lysates were prepared in 0.4M perchloric acid and neutralized in 0.72M KOH and 0.6M $KHCO_3$ in the presence of 5 mM LiCl. The lysates were then applied to Dowex columns (AG1-X8; Bio-Rad), washed, and eluted. The eluates were counted in a liquid scintillation counter. IP_3 releasing was estimated by determining the ratio of inositol phosphate radioactivity to the sum of total inositol phosphate.

Echocardiography Analyses and Hemodynamic Measurements

Transthoracic echocardiography was performed by animal specific instrument (Visual Sonics® Vevo770®, VisualSonics Inc. Canada). Mice were anesthetized and M-mode images of the left ventricle were record when mice partially recovered from anesthesia. The anterior and posterior wall thickness of left ventricular (LVAWD, LVPWD) at end-diastole and papillary muscle level was measured by two-dimensional short-axis views of the left ventricle and M-mode tracings. Left ventricle ejection fraction (LVEF) was obtained using Simpson approach. Left ventricular hemodynamics was also evaluated at 2 weeks after TAC. Briefly, a micronanometer catheter (Millar 1.4F, SPR 835, Millar Instruments, Houston, TX, USA) was inserted through the right common carotid artery into the aorta and carefully introduced into left ventricular. Left ventricular end systolic pressure (LVSBP) was measured as previously described [6].

Statistical Analysis

All data were expressed as means ± s.e.m. The between-group comparisons of means were done by one-way ANOVA followed by Tukey-Kramer test. *P* values smaller than 0.05 were considered statistical significance.

Results

RGS4 failed to inhibit mechanical stretch-induced ERK1/2 phosphorylation

Increasing evidence implicated that AT1-R could function through a heterotrimeric G-protein coupling or a G-protein-independent mode [18–20]. AngII, as the receptor agonist, activated AT1-R via a traditional GTP analog sensitive pathway. Ligand binding to G-protein-coupled receptors (GPCRs) induced GTP binding to the Gα subunit and dissociation from the βγ subunits. Here, we tested the possibility of Gα subunit activation during the process of mechanical stretch-induced AT1-R activation. It was reported that RGS4 negatively regulated Gαq signaling though promoting the hydrolysis of GTP [19,20]. Thus, the effect of Gαq coupling was attenuated by overexpressing RGS4 in cardiomyocytes. As shown in Figure 1A, Gαq-dependent phosphorylation of ERK1/2 was significantly reduced in AngII

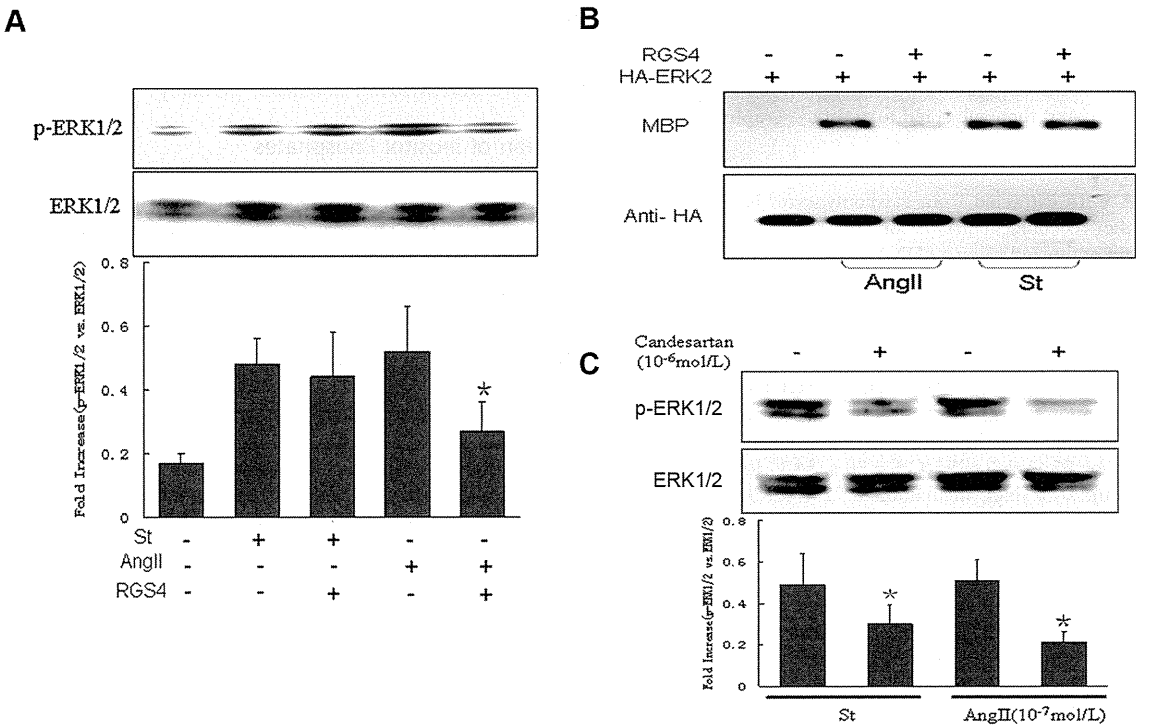

Figure 1. Mechanical stretch induced ERK1/2 signaling via activation of AT1-R, but not affected by G protein inhibition. (**A**) In vitro cultured cardiomyocytes were transfected with or without RGS4 plasmid, and then stimulated by stretch or AngII (10^{-7} mol/L) for 10 min, total proteins were collected and the expressions of phosphorylated ERK1/2 and total ERK1/2 were determined by Western blotting. (**B**) HA-tagged ERK2 was co-transfected with RGS4 plasmid into HEK-293 AT1 expressed cells for 24 h, ERK2 activity (indicated by MBP expression) was detected in cells induced by stretch or AngII, respectively. (**C**) Cardiomyocytes were pretreated with candesartan (10^{-6} mol/L) and then induced by stretch or AngII for 10 min, the expressions of phosphorylated ERK1/2 and total ERK1/2 were determined. * $P<0.05$ vs. stretch-induced group (n = 3 separated experiments).
doi:10.1371/journal.pone.0092926.g001

(10^{-7} mol/L)-induced cardiomyocytes after overexpressing RGS4. In contrast, RGS4 induced suppression of ERK1/2 was largely prevented by mechanical stretch.

To confirm the role of AT1-R in mechanical stretch evoked signal transduction, we then co-transfected HA-tagged ERK2 with RGS4 in HEK-293-AT1 expressed cells. After transient transfection for 24 h, the cells were stimulated by AngII (10^{-7} mol/L) and mechanical stretch, respectively. Immunoblotting analyses showed that ERK2 phosphorylation (indicated by MBP activity) was markedly attenuated in RGS4 overexpressed cells followed by AngII induction but not by mechanical stretch (Fig. 1B). Of note, both stretch-induced and AngII-stimulated ERK1/2 activation were inhibited by candesartan (10^{-6} mol/L) (Fig. 1C), indicating a critical role of AT1-R in regulating ERK1/2 phosphorylation during mechanical stretch.

Mechanical stretch-induced ERK1/2 phosphorylation did not depend on Gα coupling pathway

Previous in vivo studies showed that mechanical stretch-induced ERK1/2 activation was significantly attenuated in hearts from β-arrestins KO mice [7,18]. To explore whether mechanical stretch induced ERK1/2 response via β-arrestin-dependent pathway or Gα-dependent signaling, we first determined the release of inositol 1,4,5-triphosphate (IP_3) in stretch-induced cardiomyocytes, since CAMP-dependent IP_3 bioactivity was the major event of GPCRs activation through Gα protein coupling. As shown in Figure. 2A, IP_3 release was significantly attenuated in stretching-induced cardiomyocytes compared with that in AngII (10^{-7} mol/L)-induced cardiomyocytes. Both AngII and mechanical stretch mediated IP_3 release were blocked by candesartan (10^{-6} mol/L), suggesting that AT1 receptor was essential for Gα protein coupling. In addition, inhibition of PKC with GF109203X, a specific PKC inhibitor, effectively attenuated AngII (10^{-7}M) induced ERK1/2 phosphorylation, but the phosphorylation level of ERK1/2 stimulated by stretching was not affected (Fig. 2B). These data suggested that mechanical stretch mediated ERK1/2 signal might not through activating the "classical" G-protein-dependent pathway.

Next, we examined the role of β-arrestin in ERK1/2 activation induced by mechanical stretch. Results showed that both the mRNA and protein levels of β-arrestin1/2 remained unchanged in response to mechanical stretch (Fig. 2C). However, knocking down endogenous β-arrestin1/2 caused a significant decrease in the phosphorylation level of ERK1/2 in response to mechanical stretch (Fig. 2D). We further found that a robust increase of phosphorylated ERK1/2 at 10 min after stretching, which was induced by β-arrestin2 but not by β-arrestin1 in β-arrestin1 or 2 single transfected HEK-293-AT1 cells after knocking down the endogenous β-arrestin1/2 with specific siRNA (Fig. 2E).

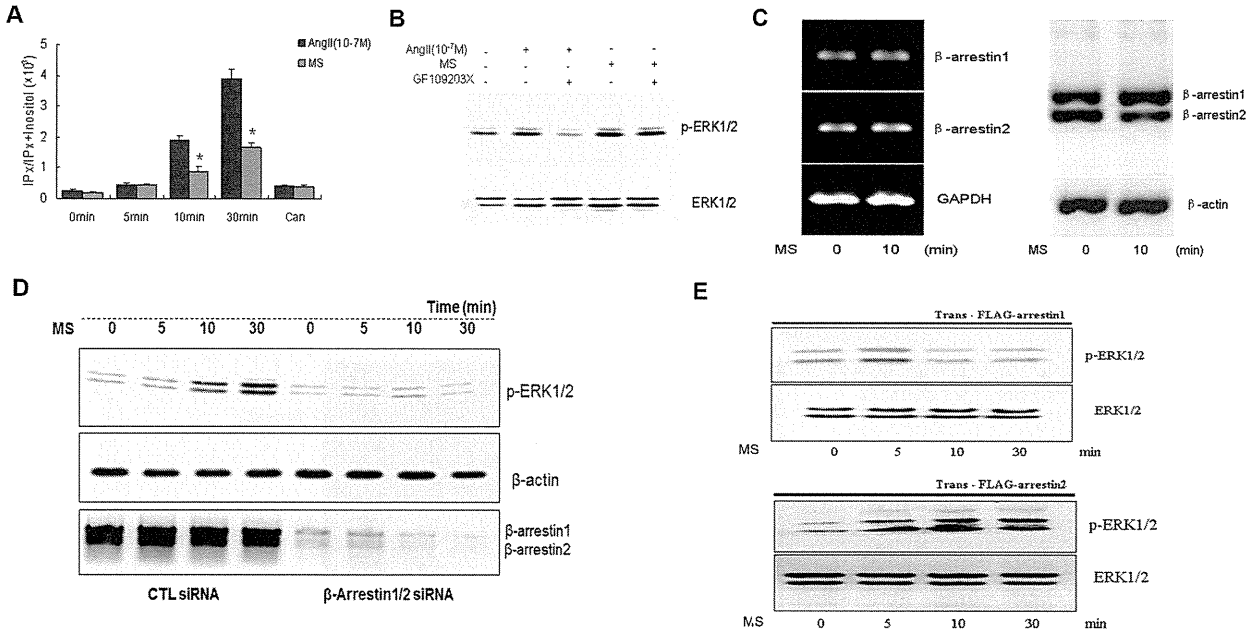

Figure 2. Mechanical stretch preferentially activated a heterotrimeric G protein-independent AT1 signaling pathway. (**A**) In vitro cultured cardiomyocytes were seeded on 24 well plates (1.5×10^5 cells) and labeled by myo-[^{3}H] inositol (1.0 μCi/mL) at 37°C for 24 h. Inositol phosphates (IPx) release was determined at the different indicated time points triggered by AngII (10^{-7} mol/L) or stretch respectively, and including the treatment of candesartan. (**B**) The effect of GF109203X on ERK1/2 phosphorylation stimulated by stretch or AngII (10^{-7} mol/L). (**C**) The endogenous mRNA and protein levels of β-arrestin1 and β-arrestin2 in cardiomyocytes were determined before and after stretch for 10 min. (**D**) Time-dependent ERK1/2 phosphorylation was determined after treatment with β-arrestin1/2 siRNA or scrambled siRNA. (**E**) Mechanical stretch-induced expression of phosphorylated ERK1/2 was determined in a single plasmid (β-arrestin1 or β-arrestin2) transfected HEK-293-AT1 cells after knock-down of endogenous β-arrestin1/2. * $P<0.05$ vs. AngII-induced group (n = 3 separated experiments).
doi:10.1371/journal.pone.0092926.g002

β-arrestin2 regulated ERK1/2 phosphorylation through interacting with the tyrosine kinase Src during mechanical stretch

Above data indicated that β-arrestin2 was critically involved in mechanical stretch-induced ERK1/2 phosphorylation, however, both mRNA and protein levels of β-arrestin2 were not affected by stretching, but the phosphorylation level of Src was suppressed by knocking down of β-arrestin2 (Fig. 3A). Therefore, we assumed that β-arrestin2 might be the scaffold protein that mediated AT1-R-dependent tyrosine kinase phosphorylation. In the Co-IP analysis, we revealed that Src was immunoprecipitated by anti-AT1-R antibody in a time dependent manner (Fig. 3B), suggesting that Src was recruited to the cell membrane and interact with AT1-R during stretching. Our previous observation indicated that one kind of Src family tyrosine kinase was critically involved in mechanical stretch-evoked AT1-R signaling [3], but a direct interaction between Src and β-arrestin2 had not been demonstrated in the model of mechanical stretch. Hence, we co-transfected FLAG-tagged β-arrestin2 and HA-tagged Src into HEK-293-AT1 cells. Afterwards, co-immunoprecipitation assays were conducted in stretched or unstretched HEK-293-AT1 cells. The proteins were collected after stretching for 10 min, and followed by immunoprecipitation of β-arrestin2 with anti-FLAG antibody. We probed the immunoprecipitated sample by Western blotting using anti-HA antibody. The results showed that β-arrestin2 interacted with Src only in stretched cells (Fig. 3C), suggesting that AT1-R mediated recruitment of β-arrestin2 might be important for Src binding and activation. But Src kinase was markedly reduced in sample from cells transfected with dominant negative β-arrestin2-V54D (Fig. 3C). Previous studies reported that β-arrestin, which functioned as a scaffold protein, could recognize and interact with the catalytic domain of Src, by which regulated its kinase activity. Therefore, the attenuated interaction between Src and β-arrestin2-V54D might be due to the lack of binding site for SH2 domain kinase docking [25]. Cell immunofluorescence further confirmed that Src kinase was phosphorylated and recruited to membrane by accumulated β-arrestin2 after mechanical stretch, but this effect was abolished by mutating the Src binding site in β-arrestin2-V54D transfected cardiomyocytes (Fig. 3D). Taken together, these data suggested that mechanical stretch-induced translocation of β-arrestin2 was essential for Src docking and signal transduction. To further investigate the effect of β-arrestin2/Src interaction after stretching on cardiomyocyte hypertrophy, we examined stretch-induced ERK1/2 phosphorylation in both β-arrestin2 and β-arrestin2-V54D transfected cardiomyocytes. The results showed that ERK1/2 phosphorylation was significantly attenuated in cells transfected with β-arrestin2-V54D compared with that in β-arrestin2 transfected cells (Fig. 3E). In addition, mechanical stretch-induced ERK1/2 activation was also inhibited by pretreating cardiomyocytes with SU6656 (10 μmol/L), a selective Src family kinase inhibitor. Of note, the inhibitory effect of SU6656 on ERK1/2 phosphorylation was not observed in cardiomyocytes stimulated by AngII (10^{-7} mol/L) (Fig. 3F). Collectively, these data confirmed that β-arrestin2/Src interaction was uniquely involved in mechanical stretch-mediated ERK1/2 activation.

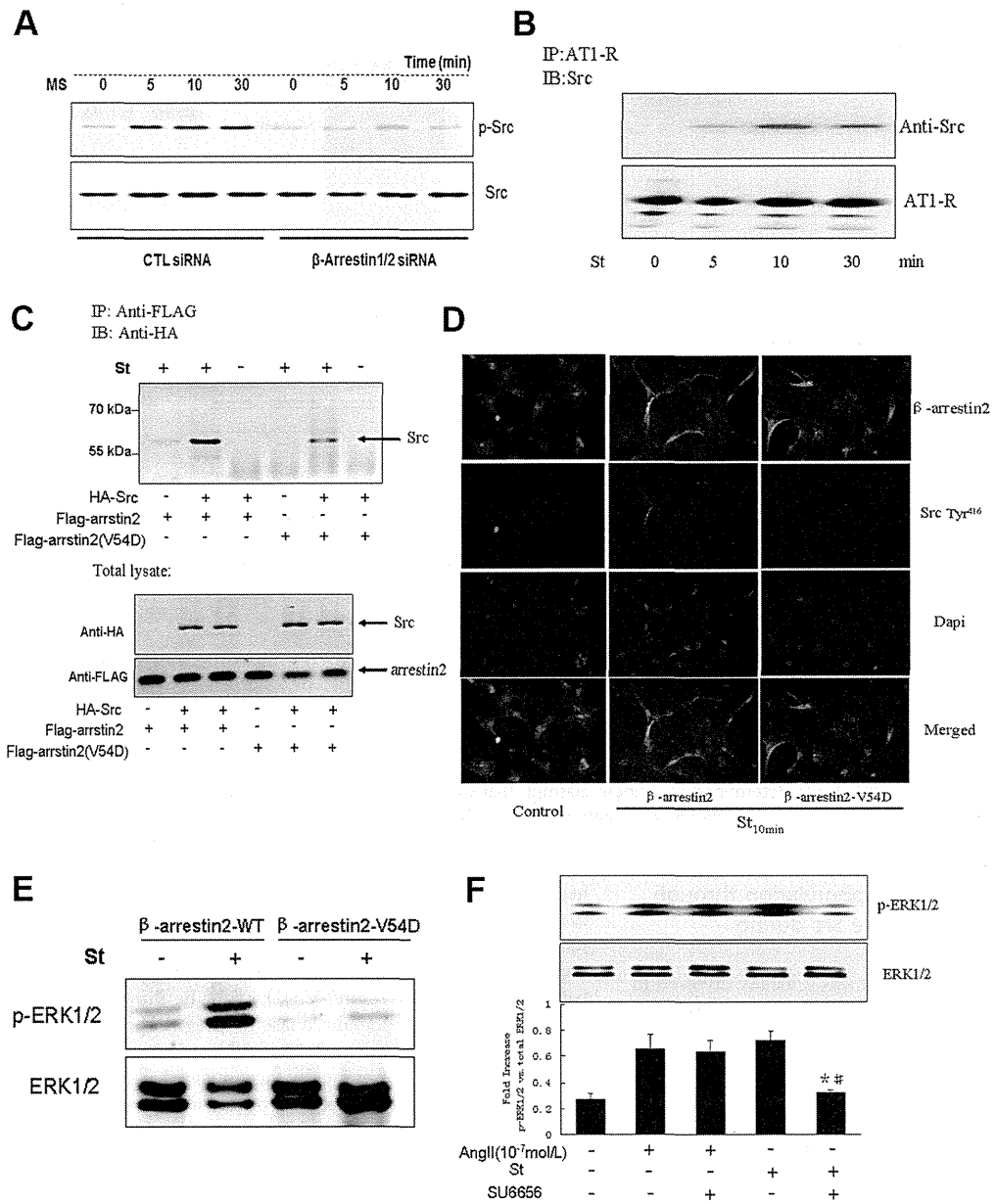

Figure 3. Src/β-arrestin2 signal complex was required for mechanical stretch-mediated AT1-R signaling. (**A**) Western blotting analyses of time-dependent Src phosphorylation after treatment with β-arrestin1/2 siRNA or scrambled siRNA. (**B**) Coimmunoprecipitation analyses of Src and AT1-R in lysates of stretched cardiomyocytes in a time-dependent manner. (**C**) HA-tagged Src and FLAG-tagged β-arrestin2 (or dominant negative β-arrestin2-V54D) were transient transfected into HEK-293-AT1 cells, whole cell extracts were immunoprecipitated with anti-FLAG monoclonal antibody, and the proteins in the immunoprecipitates and in the total lysates were probed by Western blotting using an anti-HA antibody. (**D**) The intercellular location of Src kinase in GFP-tagged β-arrestin2 WT and dominant negative GFP-tagged β-arrestin2-V54D transfected HEK-293-AT1 cells was visualized by immunofluorescence after stretching cells for 10 min. (**E**) The effect of β-arrestin2 WT or β-arrestin2-V54D transfection on mechanical stretch-induced ERK1/2 phosphorylation. (**F**) The effect of SU6656 (5 mmol/L) on ERK1/2 phosphorylation in cardiomyocytes stimulated by mechanical stretch or AngII (10^{-7} mol/L). * $P<0.05$ vs. both AngII and SU6656 treated groups; # $P<0.05$ vs. stretched groups (n = 3 separated experiments).

doi:10.1371/journal.pone.0092926.g003

Src inhibition attenuated pressure overload-induced myocardial hypertrophy

We then investigated the in vivo consequence of the inhibition of β-arrestin2/Src signaling on pressure overload-induced myocardial hypertrophy in AGT KO mice. At 2 weeks after TAC, echocardiography assessment showed a significant increase of left ventricular anterior wall at end-diastolic (LVAWd) and posterior wall at end-diastolic (LVPWd) thickerness in both C57BL/6 mice and AGT KO mice, accompanied by higher left ventricular ejection fraction (LVEF) and left ventricular end-systolic pressure (LVESP). However, Efficacy of attenuating myocardial hypertro-

phy by pretreatment with SU6656 was more pronounced in AGT KO mice than in C57BL/6 mice (Fig. 4A). Cardiac reprogramming of specific genes expressions were activated during pressure overload, we therefore determined the immediate-early response genes and fetal genes in the heart after TAC. Pressure overload enhanced the transcriptional levels of ANP, BNP and α-skeleton in AGT KO mice and C57BL/6 littermates, but expression of these re-enhanced genes was significantly lower in AGT KO mice than in C57BL/6 mice after SU6656 treatment, except for sarcoplasmic reticulum Ca^{2+}-ATPase (SERCA) (Fig. 4B).

Effects of different ARBs on AngII and TAC-induced cardiac hypertrophic response in AGT KO mice

We further compared the effects of candesartan and valsartan on myocardial hypertrophic response induced by TAC and AngII stimulation in AGT KO mice. Results showed that both candesartan and valsartan exerted inhibitory impacts on AngII-induced cardiac hypertrophy, but only candesartan effectively reversed TAC-induced hypertrophic response (Fig. 5A–B). Furthermore, Src was weakly upregulated by AngII but robustly enhanced by TAC for 2 weeks, and AngII-induced upregulation of Src was inhibited by both candesartan and valsartan, while TAC-induced Src activation was inhibited only by candesartan (Fig. 5C).

Discussion

Cardiac hypertrophy is one of the independent risk factors responsible for myocardial injury and remodeling, and such compensatory response may transit to heart failure. Plenty of previous studies have demonstrated that AT1-R is one of the most important receptors mediating cardiac hypertrophic response through multiple signaling pathways [2,3,21,22]. However, the diversity of AT1-R-mediated signaling in response to hypertrophic stimuli in the heart is still not fully understood. We have previously revealed that mechanical stretch can activate AT1-R without the involvement of AngII [3]. In this study, we further confirm a critical role of Src in regulating AT1-R-mediated intercellular signaling transduction stimulated by mechanical stretch.

Immerging evidences indicated that activation model of GPCRs might undergo different phases due to different stimuli. It was generally believed the first phase of AT1-R activation was G-protein coupling dependent, and this process was hypersensitive to ligand binding. G-protein signaling subtype 4 (RGS4), an

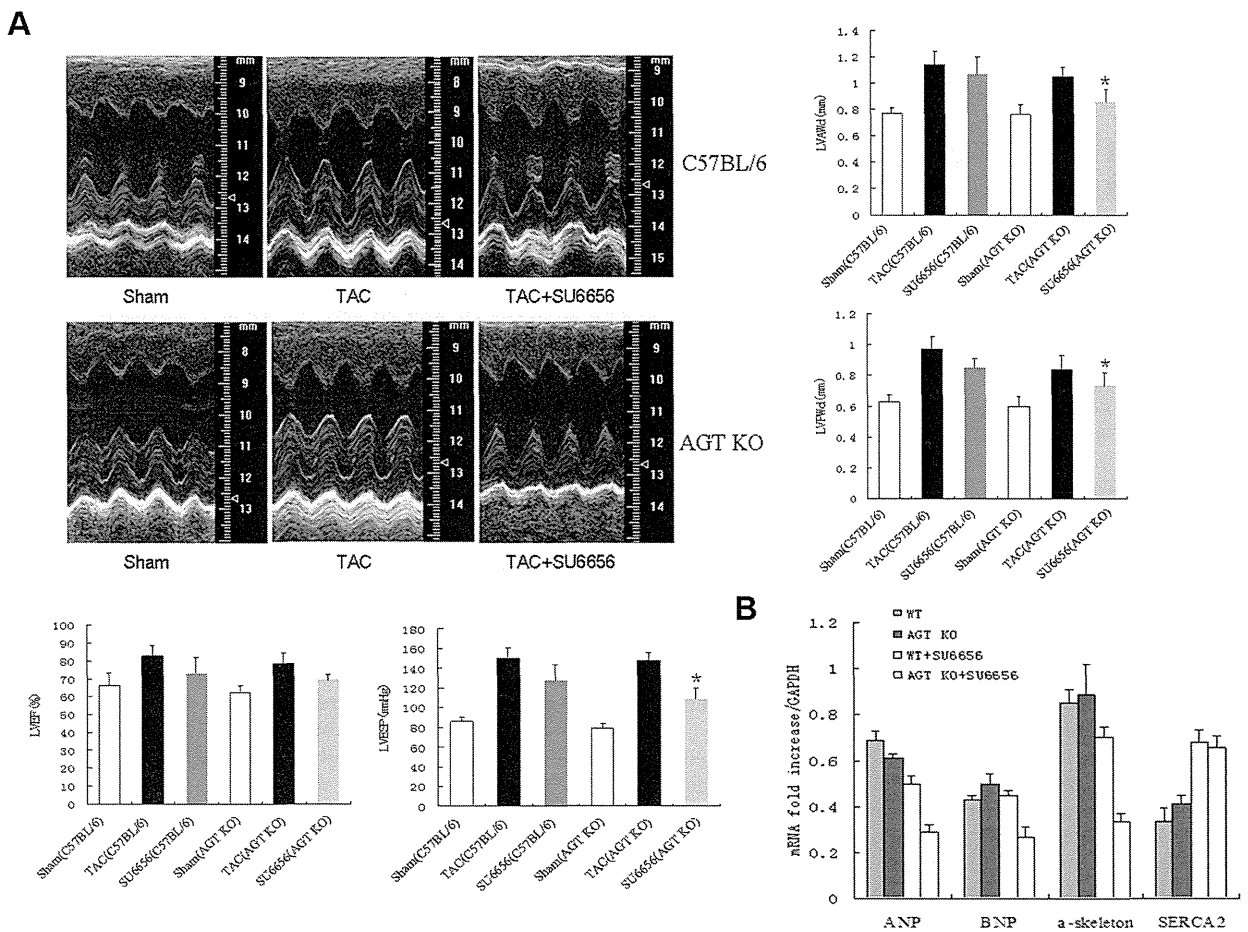

Figure 4. In vivo analyses of the cardiac function by echocardiography and hemodynamic measurements. Both AGT KO mice and the C57BL/6 WT littermates were pretreated with or without Src kinase inhibitor (SU6656), followed by TAC for 2 weeks. (**A**) Quantifications of LVAWd, LVPWd, LVEF and LVESP by representative M-mode tracing and hemodynamic recording from five mice. (**B**) Quantifications of cardiac immediate-early response genes in C57BL/6 mice and AGT KO mice with or without pretreatment of SU6656 (n = 5 separated experiments). * $P<0.05$ vs. saline-treated TAC-operated AGT KO mice.
doi:10.1371/journal.pone.0092926.g004

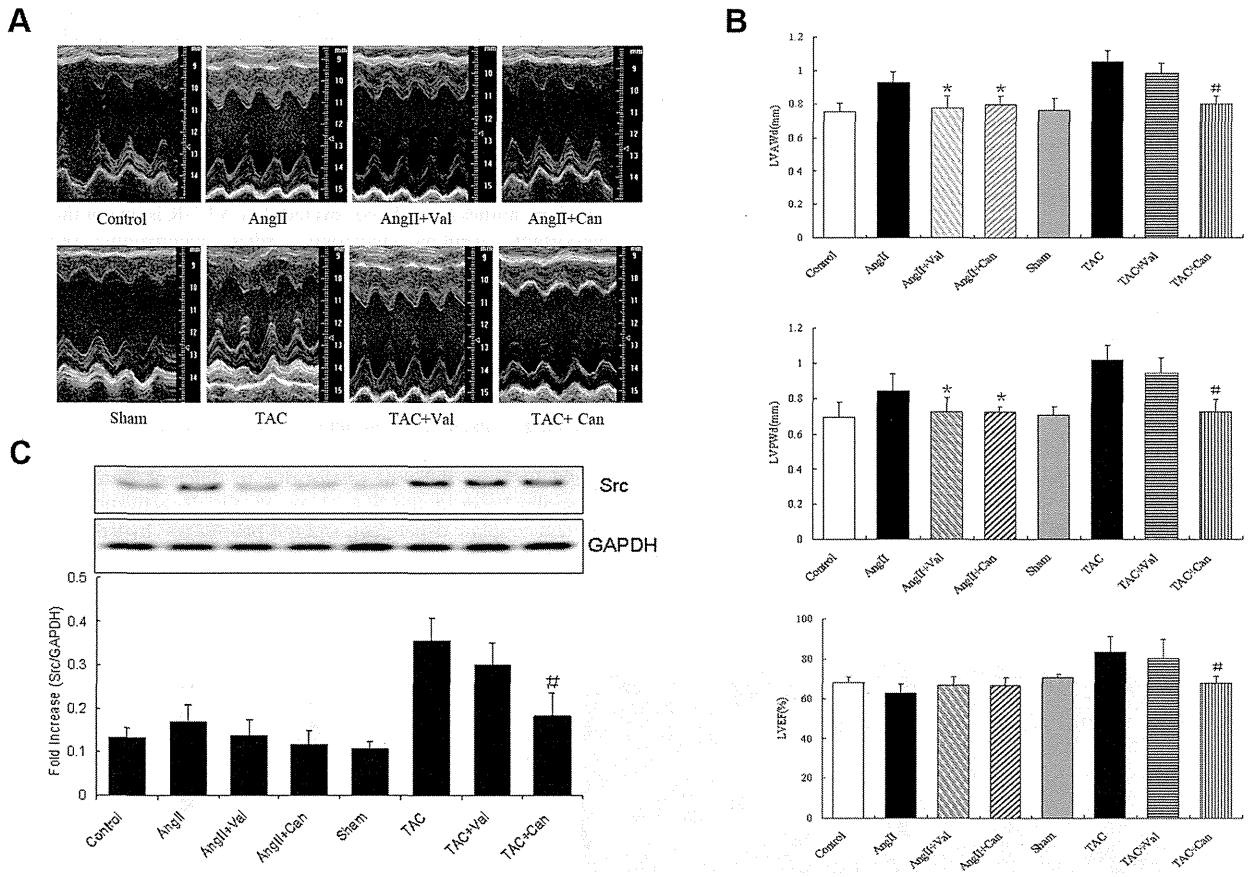

Figure 5. The effects of different ARBs on the cardiac function and Src expression in AGT KO mice. AGT KO mice were induced by AngII or TAC for 2 weeks with or without the pretreatment of valsartan or candesartan. (**A**) Representative M-mode tracings of AGT KO hearts stimulated by AngII (10^{-5} mol/L, top line) or by TAC for 2 weeks (bottom line). (**B**) Representative recording of LVAWd, LVPWd and LVEF in AGT KO mice from each group. (**C**) The expression of Src in myocardium of AGT KO mice from each group was determined. Data were presented as mean ± s.e.m. from five to eight mice. * $P<0.05$ vs. AngII-treated AGT KO mice; # $P<0.05$ vs. TAC-treated AGT KO mice.
doi:10.1371/journal.pone.0092926.g005

inhibitory regulator of GPCR signaling through accelerating GTPase activity, was mainly expressed on cardiomyocytes [23,24]. In this study, intervention of G-protein coupling by overexpressing RGS4 in cardiomyocytes effectively blocked AngII-stimulated ERK1/2 phosphorylation, the indicator of hypertrophic response, but this effect was almost invisible in mechanical stretched cardiomyocytes. These resgults suggested that stretch-mediated AT1-R activation in the absence of the ligand binding might be sensitive to a second phase of G-protein signaling transduction which was independent of G-protein coupling.

Previous studies illustrated that PKC and IP_3, two important molecules were required for AngII-mediated modulation of myofilament calcium sensitivity and cardiac excitation-contraction coupling [17,25]. However, IP_3 was not fully activated in cardiomyocytes by short time effect of mechanical stretch. Interestingly, MS-induced ERK1/2 phosphorylation was not, suppressed by blocking PKC, suggesting a G-protein coupling independent signaling pathway was involved in stretching-induced cardiac hypertrophy. Of note, SU6656, a Src kinase inhibitor, effectively suppressed stretching-induced ERK1/2 activation, indicating a crucial role of Src but not PKC was required for mechanical stretch-mediated AT1 activation and intracellular signaling.

Rakesh K. previously reported that mechanical stretch evoked an abundant increase of ERK1/2 phosphorylation in hearts from WT mice, but not from AT1-R KO or arrestin2 KO mice [7]. It was believed that distinct conformational states of AT1-R might selectively stimulate signaling via G-protein dependent or independent pathway, while β-arrestin–biased agonism might serve as the central mechanism for mechanical stretch-mediated GPCR signaling, In line with this finding, our data suggested that β-arrestin2 not β-arrestin1 was required for stretch-induced ERK1/2 phosphorylation. However, both mRNA and protein levels of β-arrestin2 remained unchanged after mechanical stretch. Instead, stretch triggered β-arrestin2 translocation to the membrane of cardiomyocyte. Previous reports indicated the divergent roles of β-arrestin1 and β-arrestin2 in regulating intercellular signal via translocation to nucleus and cell surface [16,18,26,27]. In this study, we revealed that β-arrestin2 was highly expressed on cell membrane suggesting that mechanical stretch promoted the membrane recruitment of β-arrestin2 and binding with AT1-R. Plenty of studies demonstrated that GPCRs-mediated β-arrestin2 recruitment was essential not only for receptor internalization, but also for signal transduction [18,26]. It was also proved that tyrosine kinases-dependent signal cascade was crucial for GPCRs mediated ERK1/2 phosphorylation through transactivating

EGFR [7,27,28]. However, the underlying mechanism was not yet fully clear. Our data demonstrated that AT1-R-mediated accumulation of Src kinase in response to mechanical stretch was β-arrestin2 dependent, dominant negative β-arrestin2 greatly attenuated Src docking and accumulation after stretching. Recruitment of Src to activated GPCRs had multiple functions, such as MAP kinase activation, receptor internalization, and granule release [29,30]. In our study, Src activation was essential for β-arrestin2-mediated ERK1/2 phosphorylation. Transfection with mutant β-arrestin2 V54D or inhibition of Src by SU6656 in cardiomyocytes effectively suppressed MS-induced ERK1/2 activation. Src-dependent Ras-ERK1/2 pathway was also reported in the activation of AT1a-i2m receptor, which lacking the binding site for G-protein [9,10]. Therefore, we proposed that β-arrestin2-mediated Src activation might play an important role in G-protein-independent AT1-R activation and subsequent hypertrophic response.

The activation of cellular oncogenes such as c-myc and c-Src were critically involved in the reprogram progress of gene expression during pressure overload-induced myocardial hypertrophy [31]. Here, we also found enhanced that cardiac reprogramming genes were enhanced in the pressure overload model of AGT KO mice, which indicated that AngII binding signal was not essential for regulation of fetal genes reprogramming and hypertrophy induced by mechanical stretch. Instead, inhibition of Src effectively suppressed the transcripts of ANP, BNP and α-skeleton, reversed the ventricular remodeling and hypertrophic response. In this study, we also found that mechanical stress-induced ERK1/2 response could only be suppressed by candesartan, one kind of inverse agonism, but not by valsartan.. Of note, candesartan inhibited the AT1-R activation through binding two domains of Gln257 in TM6 and Thr287 in TM7, both located at the carboxyl of the receptor, thereby stabilized AT1-R in the inactive state [4,32]. Previous studies suggested that the carboxyl-terminal residues of AT1-R were required for G-protein independent signal transduction and transactivation of EGFR [28,33]. Mutation of the conserved YIPP motif in the C terminus of AT1-R, resulted in diminished EGFR transactivation and cardiac hypertrophy in Tg-Y319F mice [33]. Because β-arrestin2-dependent Src recruitment was critically involved in GPCRs-mediated EGFR transactivation, the data presented here further supported the notion that the special effect of candesartan on mechanical stretch-induced ERK1/2 phosphorylation was achieved via inhibition of G-protein independent but β-arrestin2 dependent Src recruitment.

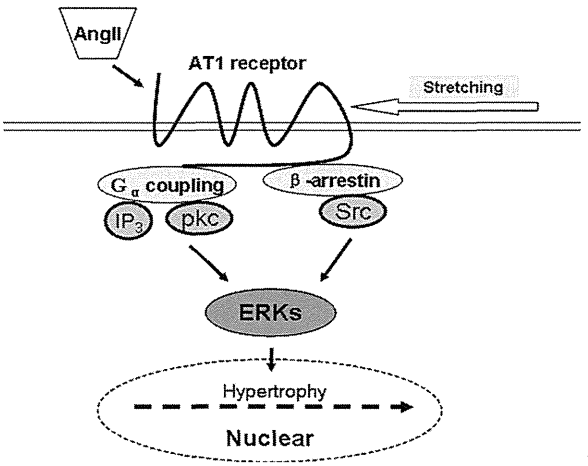

Figure 6. Schema for the mechanism of cardiac hypertrophy via AT1-R-dependent signaling pathway induced by AngII or mediated by mechanical stretch, respectively.
doi:10.1371/journal.pone.0092926.g006

In summary, our study presented the divergent mechanisms for mechanical stretch- and AngII-mediated β-arrestin2-dependent and G-protein coupling-dependent signaling pathway in cardiac hypertrophy. Mechanical stretch-induced conformational switch of AT1-R might be different from that stimulated by AngII, thus resulted in different signal transduction (Fig. 6). The uncovering of β-arrestin2/Src-mediated ERK1/2 phosphorylation in response to mechanical stretch might be crucial for the establishment of pressure overload-induced cardiac hypertrophy, and clarification of this novel mechanism might be helpful for the development of more potent inverse agonist for AT1-R.

Acknowledgments

We thanked Professor Weidong Zhu (Department of Cardiology, Shanghai East hospital, Tongji University) for helpful discussion and technical assistance.

Author Contributions

Conceived and designed the experiments: YZ SW HG. Performed the experiments: SW GJ YY JW. Analyzed the data: SW JY. Contributed reagents/materials/analysis tools: GZ IK JG. Wrote the paper: SW YZ. Helped to complete the response work and gave suggestions for study: AS.

References

1. Murphy TJ, Alexander RW, Griendling KK, Runge MS, Bernstein KE (1991) Isolation of a cDNA encoding the vascular type-1 angiotensin II receptor. Nature 351: 233–236.
2. Lorell BH (1999) Role of angiotensin AT1, and AT2 receptors in cardiac hypertrophy and disease. Am J Cardiol 83: 48H–52H.
3. Zou Y, Akazawa H, Qin Y, Sano M, Takano H, et al. (2004) Mechanical stress activates angiotensin II type 1 receptor without the involvement of angiotensin II. Nat Cell Biol 6: 499–506.
4. Yasuda N, Akazawa H, Qin Y, Zou Y, Komuro I (2008) A novel mechanism of mechanical stress-induced angiotensin II type 1-receptor activation without the involvement of angiotensin II. Naunyn Schmiedebergs Arch Pharmacol 377: 393–399.
5. Akazawa H, Yasuda N, Komuro I (2009) Mechanisms and functions of agonist-independent activation in the angiotensin II type 1 receptor. Mol Cell Endocrinol 302: 140–147.
6. Li L, Zhou N, Gong H, Wu J, Lin L, et al. (2010) Comparison of angiotensin II type 1-receptor blockers to regress pressure overload-induced cardiac hypertrophy in mice. Hypertens Res 33: 1289–1297.
7. Rakesh K, Yoo B, Kim IM, Salazar N, Kim KS, et al. (2010) beta-Arrestin-biased agonism of the angiotensin receptor induced by mechanical stress. Sci Signal 3: ra46.
8. Godin CM, Ferguson SS (2012) Biased agonism of the angiotensin II type 1 receptor. Mini Rev Med Chem 12: 812–816.
9. Zhai P, Yamamoto M, Galeotti J, Liu J, Masurekar M, et al. (2005) Cardiac-specific overexpression of AT1 receptor mutant lacking G alpha q/G alpha i coupling causes hypertrophy and bradycardia in transgenic mice. J Clin Invest 115: 3045–3056.
10. Seta K, Nanamori M, Modrall JG, Neubig RR, Sadoshima J (2002) AT1 receptor mutant lacking heterotrimeric G protein coupling activates the Src-Ras-ERK pathway without nuclear translocation of ERKs. J Biol Chem 277: 9268–9277.
11. Zhou N, Li L, Wu J, Gong H, Niu Y, et al. (2010) Mechanical stress-evoked but angiotensin II-independent activation of angiotensin II type 1 receptor induces cardiac hypertrophy through calcineurin pathway. Biochem Biophys Res Commun 397: 263–269.
12. Pullamsetti SS, Berghausen EM, Dabral S, Tretyn A, Butrous E, et al. (2012) Role of Src tyrosine kinases in experimental pulmonary hypertension. Arterioscler Thromb Vasc Biol 32: 1354–1365.

13. Reineke EL, York B, Stashi E, Chen X, Tsimelzon A, et al. (2012) SRC-2 coactivator deficiency decreases functional reserve in response to pressure overload of mouse heart. PLoS One 7: e53395.
14. Boutahar N, Guignandon A, Vico L, Lafage-Proust MH (2004) Mechanical strain on osteoblasts activates autophosphorylation of focal adhesion kinase and proline-rich tyrosine kinase 2 tyrosine sites involved in ERK activation. J Biol Chem 279: 30588–30599.
15. Chen P, Li F, Xu Z, Li Z, Yi XP (2013) Expression and distribution of Src in the nucleus of myocytes in cardiac hypertrophy. Int J Mol Med 32: 165–173.
16. Kobayashi H, Narita Y, Nishida M, Kurose H (2005) Beta-arrestin2 enhances beta2-adrenergic receptor-mediated nuclear translocation of ERK. Cell Signal 17: 1248–1253.
17. Zou Y, Komuro I, Yamazaki T, Aikawa R, Kudoh S, et al. (1996) Protein kinase C, but not tyrosine kinases or Ras, plays a critical role in angiotensin II-induced activation of Raf-1 kinase and extracellular signal-regulated protein kinases in cardiac myocytes. J Biol Chem 271: 33592–33597.
18. Rajagopal K, Whalen EJ, Violin JD, Stiber JA, Rosenberg PB, et al. (2006) Beta-arrestin2-mediated inotropic effects of the angiotensin II type 1A receptor in isolated cardiac myocytes. Proc Natl Acad Sci U S A 103: 16284–16289.
19. Yan Y, Chi PP, Bourne HR (1997) RGS4 inhibits Gq-mediated activation of mitogen-activated protein kinase and phosphoinositide synthesis. J Biol Chem 272: 11924–11927.
20. Mukhopadhyay S, Ross EM (1999) Rapid GTP binding and hydrolysis by G(q) promoted by receptor and GTPase-activating proteins. Proc Natl Acad Sci U S A 96: 9539–9544.
21. Dostal DE, Baker KM (1992) Angiotensin II stimulation of left ventricular hypertrophy in adult rat heart. Mediation by the AT1 receptor. Am J Hypertens 5:276–280.
22. Sadoshima J, Izumo S (1993) Molecular characterization of angiotensin II–induced hypertrophy of cardiac myocytes and hyperplasia of cardiac fibroblasts. Critical role of the AT1 receptor subtype. Circ Res 73:413–423.
23. Tamirisa P, Blumer KJ, Muslin AJ (1999) RGS4 inhibits G-protein signaling in cardiomyocytes. Circulation 99: 441–447.
24. Tokudome T, Kishimoto I, Horio T, Arai Y, Schwenke DO, et al. (2008) Regulator of G-protein signaling subtype 4 mediates antihypertrophic effect of locally secreted natriuretic peptides in the heart. Circulation 117: 2329–2339.
25. Purdy KE, Arendshorst WJ (2001) Iloprost inhibits inositol-1,4,5-trisphosphate-mediated calcium mobilization stimulated by angiotensin II in cultured preglomerular vascular smooth muscle cells. J Am Soc Nephrol 12: 19–28.
26. Shenoy SK, Drake MT, Nelson CD, Houtz DA, Xiao K, et al. (2006) beta-arrestin-dependent, G protein-independent ERK1/2 activation by the beta2 adrenergic receptor. J Biol Chem 281: 1261–1273.
27. Kim J, Ahn S, Rajagopal K, Lefkowitz RJ (2009) Independent beta-arrestin2 and Gq/protein kinase Czeta pathways for ERK stimulated by angiotensin type 1A receptors in vascular smooth muscle cells converge on transactivation of the epidermal growth factor receptor. J Biol Chem 284: 11953–11962.
28. Noma T, Lemaire A, Naga Prasad SV, Barki-Harrington L, Tilley DG, et al. (2007) Beta-arrestin-mediated beta1-adrenergic receptor transactivation of the EGFR confers cardioprotection. J Clin Invest 117: 2445–2458.
29. Luttrell LM, Ferguson SS, Daaka Y, Miller WE, Maudsley S, et al. (1999) Beta-arrestin-dependent formation of beta2 adrenergic receptor-Src protein kinase complexes. Science 283: 655–661.
30. Miller WE, Maudsley S, Ahn S, Khan KD, Luttrell LM, et al. (2000) beta-arrestin1 interacts with the catalytic domain of the tyrosine kinase c-SRC. Role of beta-arrestin1-dependent targeting of c-SRC in receptor endocytosis. J Biol Chem 275: 11312–11319.
31. Komuro I, Kurabayashi M, Takaku F, Yazaki Y (1988) Expression of cellular oncogenes in the myocardium during the developmental stage and pressure-overloaded hypertrophy of the rat heart. Circ Res 62: 1075–1079.
32. Zhai P, Galeotti J, Liu J, Holle E, Yu X, et al. (2006) An angiotensin II type 1 receptor mutant lacking epidermal growth factor receptor transactivation does not induce angiotensin II-mediated cardiac hypertrophy. Circ Res 99: 528–536.
33. Yasuda N, Miura S, Akazawa H, Tanaka T, Qin Y, et al. (2008) Conformational switch of angiotensin II type 1 receptor underlying mechanical stress-induced activation. EMBO Rep 9: 179–186.
34. Zhang P, Xu D, Wang S, Fu H, Wang K, et al.(2011) Inhibition of aldehyde dehydrogenase 2 activity enhances antimycin-induced rat cardiomyocytes apoptosis through activation of MAPK signaling pathway. Biomed Pharmacother. 65:590–593.

nature genetics

Recurrent gain-of-function mutations of *RHOA* in diffuse-type gastric carcinoma

Miwako Kakiuchi[1,2], Takashi Nishizawa[3], Hiroki Ueda[1], Kengo Gotoh[1], Atsushi Tanaka[4], Akimasa Hayashi[4], Shogo Yamamoto[1,5], Kenji Tatsuno[1,5], Hiroto Katoh[6], Yoshiaki Watanabe[7], Takashi Ichimura[4], Tetsuo Ushiku[4], Shinichi Funahashi[3], Keisuke Tateishi[2], Ikuo Wada[8], Nobuyuki Shimizu[8], Sachiyo Nomura[8], Kazuhiko Koike[2], Yasuyuki Seto[8], Masashi Fukayama[4], Hiroyuki Aburatani[1,5] & Shumpei Ishikawa[1,4,6]

Diffuse-type gastric carcinoma (DGC) is characterized by a highly malignant phenotype with prominent infiltration and stromal induction. We performed whole-exome sequencing on 30 DGC cases and found recurrent *RHOA* nonsynonymous mutations. With validation sequencing of an additional 57 cases, *RHOA* mutation was observed in 25.3% (22/87) of DGCs, with mutational hotspots affecting the Tyr42, Arg5 and Gly17 residues in RHOA protein. These positions are highly conserved among RHO family members, and Tyr42 and Arg5 are located outside the guanine nucleotide–binding pocket. Several lines of functional evidence indicated that mutant RHOA works in a gain-of-function manner. Comparison of mutational profiles for the major gastric cancer subtypes showed that *RHOA* mutations occur specifically in DGCs, the majority of which were histopathologically characterized by the presence of poorly differentiated adenocarcinomas together with more differentiated components in the gastric mucosa. Our findings identify a potential therapeutic target for this poor-prognosis subtype of gastric cancer with no available molecularly targeted drugs.

Gastric cancer is one of the most frequent causes of cancer-related mortality in the world[1], with the highest incidence occurring in East Asia, Central and Eastern Europe, and South Africa in particular[2]. Among various types of gastric cancer, DGC represents a subtype with poor prognosis[3–6]; as a result, DGC has gained substantial public attention worldwide. DGC is histologically characterized as a poorly differentiated adenocarcinoma in which single isolated cancer cells or small collective masses of cancer cells massively infiltrate into adjacent tissue in a highly invasive manner with prominent scirrhous stromal reactions. So far, a couple of molecularly targeted drugs have been developed against gastric cancer, including HER2 antagonists. In the intestinal type of gastric cancer, the most common type, approximately 30% of tumors show positivity for HER2 protein expression; however, only fewer than 10% of DGC tumors show positivity for HER2[7,8]. Thus, DGC constitutes a poor-prognosis subgroup of gastric cancer with no known effective molecularly targeted therapies. Recent genomic characterization of gastric cancer by whole-exome sequencing showed that a large number of known cancer-related genes are frequently mutated in gastric malignancies: Wang *et al.* reported frequent mutations in *TP53*, *PTEN*, *ARID1A*, *APC*, *CTNNB1*, *CDH1* and other genes[9], and Zang *et al.* identified somatic mutations in *TP53*, *PI3KCA*, *CTNNB1*, *ARID1A*, *KMT2C* and *FAT4*, among other genes[10]. However, most of the sequenced tumors in these studies were intestinal-type gastric cancers (IGCs). Therefore, DGC-specific molecular carcinogenesis mechanisms and druggable gene targets remain to be elucidated.

To explore driver mutations in DGC development, we performed whole-exome sequencing on 30 clinical samples of DGC that exhibited poorly differentiated cancer cells and/or signet ring cells with prominent scirrhous stroma in histological analysis. To enrich the tumor fraction relative to the dominant stromal component and other normal cells, we performed macrodissection in which areas that had relatively predominant tumor features under histopathological examination were scraped from tissue sections, eliminating normal epithelium components. Even after these procedures, our analysis estimated that the tumor content ratio ranged from 65% at the maximum to less than 20% at the minimum (**Supplementary Fig. 1**). We extracted genomic DNA from cancer tissues and corresponding normal components, and coding exon fragments were enriched by exon capture (SureSelect, Agilent Technologies) according to the manufacturer's protocol. Whole-exome sequencing was conducted using the Illumina HiSeq platform. Sequencing depths for tumors and corresponding normal components were 102× and 99× on averages, respectively, depths that are substantially greater than in typical exome studies, meaning that sufficient numbers of reads for mutant alleles could be obtained,

[1]Genome Science Division, Research Center for Advanced Science and Technology, The University of Tokyo, Tokyo, Japan. [2]Department of Gastroenterology, Graduate School of Medicine, The University of Tokyo, Tokyo, Japan. [3]Forerunner Pharma Research Co., Ltd., Tokyo, Japan. [4]Department of Pathology, Graduate School of Medicine, The University of Tokyo, Tokyo, Japan. [5]Translational Systems Biology and Medicine Initiative (TSBMI), The University of Tokyo, Tokyo, Japan. [6]Department of Genomic Pathology, Medical Research Institute, Tokyo Medical and Dental University, Tokyo, Japan. [7]Kamakura Research Laboratories, Chugai Pharmaceutical Co., Ltd., Kanagawa, Japan. [8]Department of Gastrointestinal Surgery, Graduate School of Medicine, The University of Tokyo, Tokyo, Japan. Correspondence should be addressed to S.I. (sish.gpat@mri.tmd.ac.jp).

Received 28 June 2013; accepted 14 April 2014; published online 11 May 2014; doi:10.1038/ng.2984

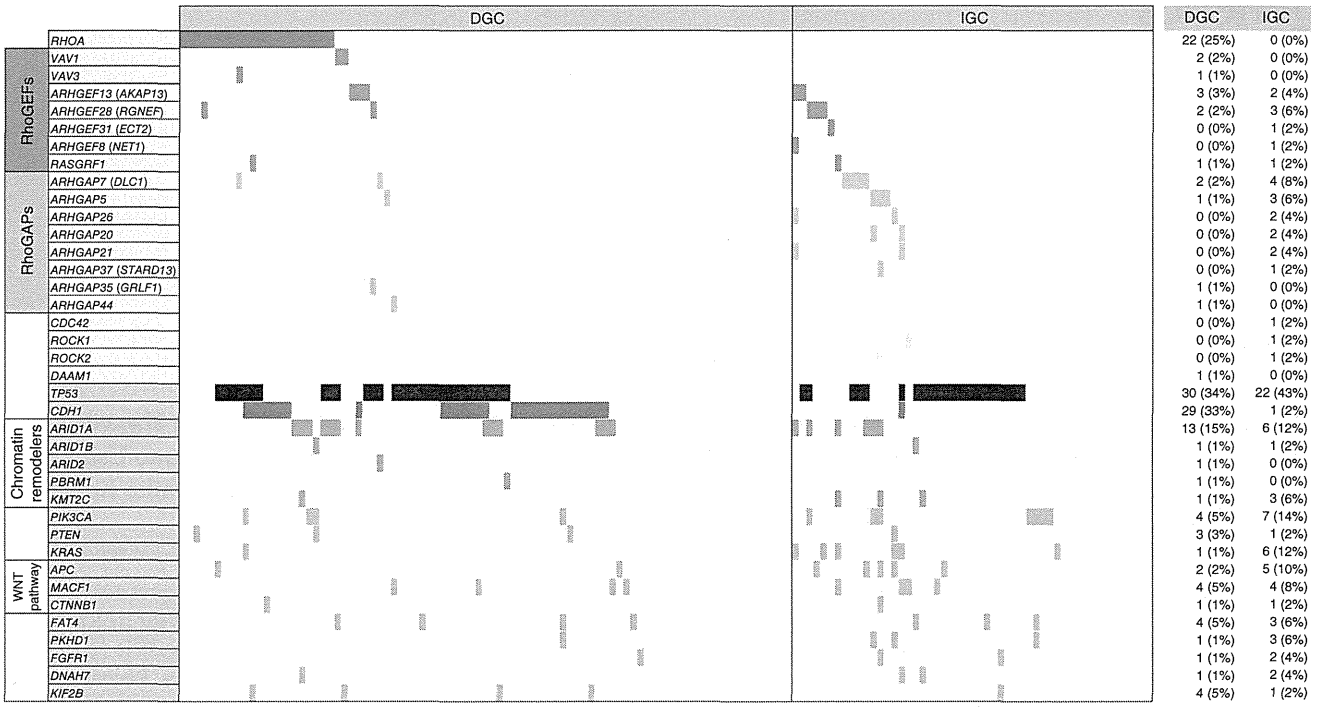

Figure 1 Landscape of genetic changes in two major subtypes of gastric cancer. Overall view of the somatic mutations in 87 DGC and 51 IGC samples. Genes closely linked to *RHOA* (yellow) or frequently mutated in the discovery screen and in previous reports[9,10] (light green) are shown. Colored cells represent somatically mutated genes: for example, *RHOA* (red), RhoGEF genes (pink) and RhoGAP genes (orange). The total numbers and percentages of the mutant cases in each subtype are shown to the right.

even from such stroma-rich background (**Supplementary Fig. 2**). We identified 6,616 somatic mutations (5,359 single-nucleotide variations (SNVs) and 1,257 indels) in the 30 DGC specimens, of which 1,838 occurred as nonsynonymous mutations (1,680 SNVs and 158 indels), with averages of 56 SNVs and 5 indels per case. (Detailed somatic mutation data in this report are available in **Supplementary Data Set 1**.) These somatic mutation frequencies in DGC are comparable to those described for IGC in previous reports. Profiles of mutations and indels suggested that none of the DGCs analyzed in this study had the MSI-H (microsatellite instability high) phenotype (**Supplementary Fig. 1**). Mutational signature analyses showed that the sequence contexts for DGC mutations were distinct from those in IGC (**Supplementary Fig. 3**), and the most characteristic T>G substitution pattern (GTG>GGG or CTT>CGT substitution was relatively frequent) was similar to a known cancer mutation signature reported by a global cancer study[11] (**Supplementary Fig. 3**), although its related etiology is still unclear. Previously known mutations[9,10] were detected in the *TTN* and *TP53* genes in 11 of 30 DGC samples, and *ARID1A* gene mutations were detected in 5 of the DGC samples. We also found nonsynonymous somatic mutations in five DGC cases in the *CDH1* gene, germline mutations of which are known to cause familial DGC[12]. Furthermore, four cases had mutations in genes encoding WNT pathway molecules such as *APC*, *MACF1* (refs. 13,14) and *CTNNB1* (**Supplementary Table 1**).

We observed recurrent somatic mutations in 23% (7/30) of DGC samples in the *RHOA* gene encoding a small GTPase, a finding not yet reported in gastric cancers (**Fig. 1**). Notably, mutation encoding p.Tyr42Cys was detected in four of the seven mutated cases. This biased distribution of mutations implies that these mutations work in a gain-of-function manner. To further investigate the precise frequency and distribution of somatic mutations in *RHOA* and 26 selected *RHOA*-related genes in DGC, we performed targeted sequencing for a validation sample set consisting of 57 independent DGC cases and the 30 cases from the discovery set. Furthermore, to more comprehensively investigate the mutational profiles of the major gastric cancer subtypes, we included 51 IGC cases in our validation screen as well as 19 additional genes (46 genes in total) that were frequently mutated in our discovery screen and have been reported to be altered in previous exome studies (Online Methods and **Supplementary Table 2**). Deep resequencing of the validation set with mean sequencing depths of 4,082× and 4,489× in cancer and corresponding normal components, respectively, identified nonsynonymous somatic mutations in the *RHOA* gene in 25.3% (22/87) of DGC cases (**Fig. 1**). These somatic mutations were unevenly distributed across the *RHOA* gene: mutational hotspots affected the Tyr42, Arg5 and Gly17 residues in the RHOA protein (**Fig. 2a**). Nucleotide substitutions causing p.Gly17Glu and p.Arg5Gln alterations were present in the dbSNP database (rs11552761 and rs11552758, respectively), but we confirmed that they were somatic in nature in our cohort (**Supplementary Fig. 2**). Other known recurrent mutations were also found in *TP53* in 34% (30/87) of cases, in *CDH1* in 32% (28/87) of cases and in *ARID1A* in 15% (13/87) of cases.

Interestingly, we found that some cases harbored nonsynonymous mutations in RhoGAP (GTPase-activating protein) or RhoGEF (GDP/GTP-exchange factor) genes (**Fig. 1**), suggesting that RHOA in combination with its regulatory molecules is frequently mutated in DGC samples (36%; 31/87 cases in our cohort). Mutations of RhoGAP or RhoGEF genes were not specific to DGC and were also observed in IGC cases. In our comparative mutational analysis of DGC and IGC samples, many of the frequent mutations, such as those in *TP53*, *PIK3CA*, WNT pathway genes (*CTNNB1* and *APC*) and chromatin-remodeling and SWI/SNF complex components (*ARID1A* and *KMT2C*), were commonly found in both DGCs and

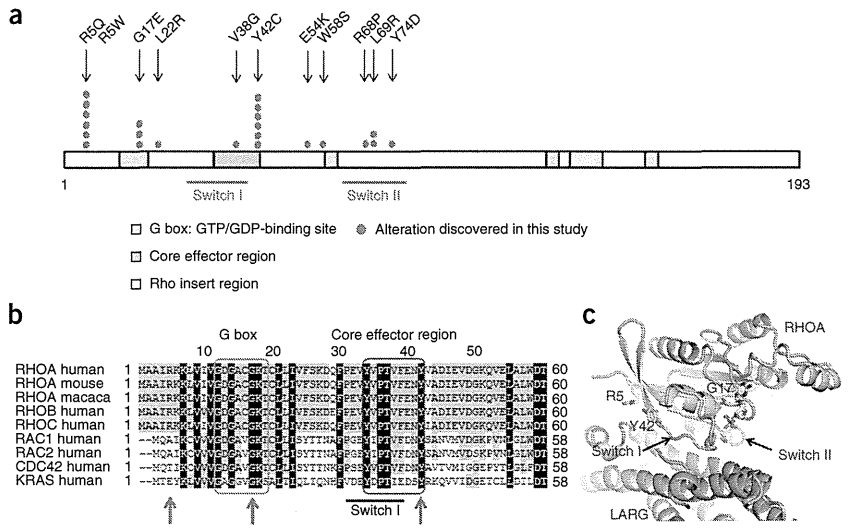

Figure 2 Distribution of RHOA alterations in DGC. (**a**) Map of RHOA functional regions and the sites of the amino acid substitutions discovered in this study. Recurrent alterations are indicated by multiple circles. (**b**) Amino acid alignment of RHOA and RHO family proteins (amino acids 1–60). The G box and core effector region are highly conserved across other mammalian RHOA and human RHO families, as highlighted by green and red boxes, respectively. Red arrows indicate the most frequently mutated positions—Arg5, Gly17 and Tyr42. (**c**) Structure of RHOA and one of its representative RhoGEF proteins, LARG, in its GDP-bound form. RHOA and LARG are shown in green and gray, respectively (Protein Data Bank (PDB) 1X86). Tyr42, one of the most frequently mutated residues in this study, is located on an interaction surface of RHOA with RhoGEFs.

IGCs. *KRAS* mutation was relatively frequent in IGCs. In sharp contrast, the somatic mutations in *RHOA* and *CDH1* were highly specific to the DGC subtype (**Fig. 1**). Frequently affected by mutation, the CDH1 and RHOA signaling pathways are reported to be functionally linked with each other[15,16], indicating that dysregulation around these two signaling pathways would contribute to DGC development (**Supplementary Fig. 4**). Immunohistochemical analyses showed that, of the *RHOA*-mutant DGC cases tested, only a small fraction (4.5%; 1/22) had positivity for HER2 staining (**Supplementary Table 3**), suggesting the possibility of using RHOA as a therapeutic target in DGCs that are not responsive to HER2-targeted therapy. The RHO family of small GTPase proteins consists of approximately 20 members, including RHOA[17], and some family members such as RAC1 have been reported to be mutated in cancers other than gastric cancer[18,19]. The RHO family is clustered as a branch of the KRAS small GTPase superfamily including RAS. The Tyr42, Arg5 and Gly17 residues in RHOA, which were identified as the most frequent sites of alteration in this study, are highly conserved among RHO family proteins (**Fig. 2**). The Tyr42 residue is located within a region called the core effector domain, an important functional domain for physical interaction with effector molecules and/or RhoGEFs and RhoGAPs in the RHOA signaling pathway (**Fig. 2b,c**).

Known biological functions of RHOA are related to actin organization[20], cell migration[21], cytokinesis and the cell cycle[22]. Although somatic mutations of *RHOA* in malignant tumors have not been reported to occur frequently, RHOA overexpression has been found in various cancers, and RHOA is also known to have a key role in tumorigenesis and in tumor cell invasion in various malignancies[23]. To investigate the consequences of the *RHOA* mutations found in DGC tumors, we performed three-dimensional cell growth assays using the OE19 cell line derived from adenocarcinoma of the gastric cardia, which harbors a nucleotide substitution in the *RHOA* gene affecting Tyr42, and the SW948 colon cancer cell line and the BT474 breast cancer cell line, which harbor *RHOA* mutations affecting a conserved Gly17 position located near a region of the protein that is important for its GTPase activity (**Fig. 2c**) (Cancer Cell Line Encyclopedia (CCLE); see URLs). Growth rates for cells from all three cell lines were obviously suppressed in three-dimensional culture by small interfering RNA (siRNA)-mediated knockdown of *RHOA* expression, implying that the *RHOA* mutations provide a strong growth advantage in DGC progression. In sharp contrast, no obvious growth suppression was observed in the AGS and MKN74 gastric cancer cell lines that have wild-type *RHOA* genes (**Fig. 3a,b**). Furthermore, we conducted gain-of-function rescue experiments using siRNA-resistant wild-type or mutant *RHOA* constructs in combination with endogenous *RHOA* knockdown. For these experiments, we used the *RHOA*-mutated SW948 cell line whose growth was strongly inhibited by knockdown of endogenous *RHOA*. Expression of siRNA-resistant Gly17Glu RHOA strongly nullified the inhibitory effect from knockdown of endogenous *RHOA* in SW948 cells, and these cells showed growth comparable to that of control cells (**Fig. 3c**). This phenomenon was replicated by introducing expression of the Tyr42Cys RHOA mutant, indicating that the p.Tyr42Cys and p.Gly17Glu substitutions, although affecting different amino acid positions, have a similar effect on DGC biology. In contrast, expression of siRNA-resistant wild-type RHOA failed to reverse the inhibitory effect from knockdown of endogenous *RHOA* (**Fig. 3c**), indicating that it is specifically the RHOA mutants that have growth-promoting effects. We did not observe similarly clear effects in the AGS and MKN74 cell lines with wild-type *RHOA* genes and in non-transformed HEK293 cells (data not shown), and we therefore speculate that the RHOA mutants work in a context-dependent manner, most likely coupled with other cancer-specific signaling, a hypothesis that is well exemplified by the *KRAS* oncogene[24]. In cancer cells with wild-type *RHOA*, the mutants would have a different mutational context, in which unidentified RHOA-related pathway(s) are possibly activated by different mechanisms. Taken together, our data demonstrate that mutant RHOA, by working in a gain-of-function manner, has a key role in DGC biology (**Supplementary Note**).

In histopathological examination of our cohort of DGC samples, 16 of 22 *RHOA*-mutant cases were classified as advanced gastric cancer with tumor cells invading deeper than the muscle layer, although this invasive feature was also observed in cases with wild-type *RHOA*. Most of these advanced cancers (75%; 12/16) were macroscopically defined as having an appearance consistent with Borrmann type 3 (ref. 25). Histologically, these tumors were defined by the presence of both poorly differentiated cancer components with extensive stromal reactions under submucosal layers and more differentiated tubular components in the mucosa (**Supplementary Fig. 5a–c**), with this heterogeneity possibly reflecting stepwise progression in DGC[26]. To examine the relationship between *RHOA* mutations and cancer progression, we performed microscope-based dissection of histologically distinct features—for example, diffuse and tubular components—from each of these tumors, and extracted DNA was sequenced

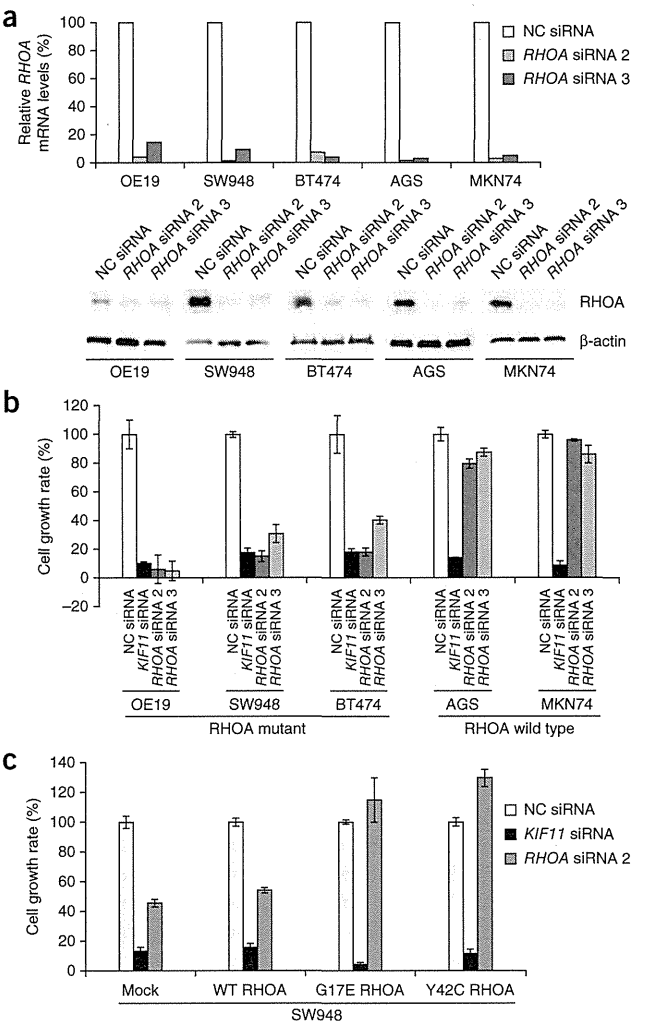

Figure 3 Functional assays for mutant RHOA proteins. (**a**,**b**) Effect of knockdown on mutant RHOA. (**a**) Efficient knockdown of RHOA mRNA and protein in all cell lines used. Top, *RHOA* knockdown was confirmed by quantitative RT-PCR. Levels of *RHOA* mRNA were normalized to *RPS18* mRNA levels (set as 100% for the negative control (NC) baseline states). Bottom, RHOA protein blots showing the efficacy of siRNA in OE19, SW948, BT474, AGS and MKN74 cells; β-actin was used as a loading control. (**b**) Growth inhibition mediated by *RHOA* knockdown in three-dimensional culture. In *RHOA*-mutant OE19, SW948 and BT474 cells, cell growth was inhibited as much as in the positive control cells treated with *KIF11* siRNA, whereas growth inhibition was hardly observed in AGS and MKN74 cells with wild-type *RHOA*. Cell growth inhibition assays were performed in triplicate; data are shown as means ± s.d. Percentages are relative to cells treated with negative control siRNA. (**c**) Gain-of-function rescue experiments for mutant RHOA proteins. SW948 cells were infected with an episome encoding either siRNA-resistant wild-type (WT), Gly17Glu or Tyr42Cys RHOA in combination with siRNA-mediated knockdown of endogenous *RHOA*. Expression of the Gly17Glu and Tyr42Cys mutants in SW948 cells nullified the growth inhibitory effects from knockdown of endogenous *RHOA*. In contrast, expression of plasmid alone (mock) or wild-type RHOA in SW948 cells did not yield such effects. Assays were performed in triplicate; data are shown as means ± s.d. Percentages are relative to cells treated with negative control siRNA.

(**Supplementary Fig. 5d–g**). In all of the samples analyzed, *RHOA* mutations were observed in both classes of tissue, suggesting that *RHOA* mutations might have a key role beginning in the initial stages of cancer progression (**Supplementary Table 4**). In our cohort, we did not find any significant difference in clinical features (stage, lymph node status or extent of metastasis) between DGCs with mutant and wild-type *RHOA*, although this finding should be confirmed by further large-scale investigations.

Previous sequencing analyses of gastric cancer have not reported *RHOA* mutations so far. This may, however, be owing to the paucity of DGC cases in the discovery sample sets of previous studies: with only two or three DGCs in a sample set, it would have been statistically difficult to identify *RHOA* mutations by screening. Furthermore, it is possible that the low tumor content in DGC tissues caused under-representation of mutant sequences in conventional analysis thus far (**Supplementary Figs. 1** and **2**).

In summary, using whole-exome sequencing and subsequent targeted deep sequencing, we herein report recurrent mutations of *RHOA* in DGC (occurring in 25.3% of the cases in our cohort). Furthermore, several functional assays implicated RHOA mutants as oncogenic drivers in DGC progression. The frequency of DGC varies across geographic areas, but DGC comprises around 30–50% of all gastric cancers according to recent reports from European countries and Japan[4,27–29]. However, despite such a relatively high frequency, *RHOA*-mutant gastric cancers cannot be optimal therapeutic applications of any known molecularly targeted antitumor drugs; for example, almost all of the DGC cases with *RHOA* mutation were HER2 negative in our cohort. Taking into consideration its structural characteristics (**Fig. 2**), RHOA could be a druggable oncogenic protein, as it has various targetable domains such as binding pockets for GTP[30] and structural regions of protein-protein interaction with effectors, RhoGAPs and RhoGEFs[31]. By specifically interfering with mutant RHOA and its oncogenic pathways, it might be possible to develop novel therapeutic strategies against otherwise devastating DGCs that undergo massive invasion and metastasis.

URLs. Cancer Cell Line Encyclopedia (CCLE), http://www.broadinstitute.org/ccle/; karkinos genotyper, http://sourceforge.net/projects/karkinos/; BioGRID, http://thebiogrid.org/; Human Protein Reference Database (HPRD), http://www.hprd.org/.

METHODS

Methods and any associated references are available in the online version of the paper.

Note: Any Supplementary Information and Source Data files are available in the online version of the paper.

ACKNOWLEDGMENTS

We would like to thank K. Shiina, K. Sakuma, K. Nakano, A. Nishimoto and R. Sato for technical assistance. This study was supported by Grants-in-Aid for Scientific Research in Innovative Areas to the "Systems Cancer Project" (grant 22134003) from the Ministry of Education, Culture, Sports, Science and Technology of Japan (S.I.), by JSPS (Japan Society for the Promotion of Science) KAKENHI grant 24221011 (H.A.), by a Health Labor Sciences Research Grant (H.A.) and by a grant for the Translational Systems Biology and Medicine Initiative (TSBMI) from the Ministry of Education, Culture, Sports, Science and Technology of Japan (S.Y., K. Tatsuno and H.A.). The supercomputing resource was provided by the Human Genome Center (University of Tokyo).

AUTHOR CONTRIBUTIONS

S.I. and H.A. designed the study. M.K. processed samples and supervised exome sequencing. H.U., K.G., K. Tatsuno and S.Y. performed computational analyses. Y.S., M.F., I.W., N.S., A.H. and S.N. coordinated sample acquisition. H.K., T.I. and T.U. carried out pathological review and analysis. A.T. performed dissection analysis. T.N. and S.F. performed functional experiments. Y.W. carried out structural analysis. S.I. wrote the manuscript. H.A., M.F., K. Tateishi and K.K. were involved in critical review and discussion.

COMPETING FINANCIAL INTERESTS
The authors declare competing financial interests: details are available in the online version of the paper.

1. Hohenberger, P. & Gretschel, S. Gastric cancer. *Lancet* **362**, 305–315 (2003).
2. Guggenheim, D.E. & Shah, M.A. Gastric cancer epidemiology and risk factors. *J. Surg. Oncol.* **107**, 230–236 (2013).
3. Kong, X., Wang, J.L., Chen, H.M. & Fang, J.Y. Comparison of the clinicopathological characteristics of young and elderly patients with gastric carcinoma: a meta analysis. *J. Surg. Oncol.* **106**, 346–352 (2012).
4. Warneke, V.S. *et al.* Cohort study based on the seventh edition of the TNM classification for gastric cancer: proposal of a new staging system. *J. Clin. Oncol.* **29**, 2364–2371 (2011).
5. Chiaravalli, A.M. *et al.* Histotype-based prognostic classification of gastric cancer. *World J. Gastroenterol.* **18**, 896–904 (2012).
6. Stiekema, J. *et al.* Surgical treatment results of intestinal and diffuse type gastric cancer. Implications for a differentiated therapeutic approach? *Eur. J. Surg. Oncol.* **39**, 686–693 (2013).
7. Tanner, M. *et al.* Amplification of HER-2 in gastric carcinoma: association with Topoisomerase IIα gene amplification, intestinal type, poor prognosis and sensitivity to trastuzumab. *Ann. Oncol.* **16**, 273–278 (2005).
8. Bang, Y. *et al.* Pathological features of advanced gastric cancer (GC): relationship to human epidermal growth factor receptor 2 (HER2) positivity in the global screening programme of the ToGA trial. *J. Clin. Oncol.* **27**, 4556 (2009).
9. Wang, K. *et al.* Exome sequencing identifies frequent mutation of *ARID1A* in molecular subtypes of gastric cancer. *Nat. Genet.* **43**, 1219–1223 (2011).
10. Zang, Z.J. *et al.* Exome sequencing of gastric adenocarcinoma identifies recurrent somatic mutations in cell adhesion and chromatin remodeling genes. *Nat. Genet.* **44**, 570–574 (2012).
11. Alexandrov, L.B. *et al.* Signatures of mutational processes in human cancer. *Nature* **500**, 415–421 (2013).
12. Guilford, P. *et al.* E-cadherin germline mutations in familial gastric cancer. *Nature* **392**, 402–405 (1998).
13. Chen, H.J. *et al.* The role of microtubule actin cross-linking factor 1 (MACF1) in the Wnt signaling pathway. *Genes Dev.* **20**, 1933–1945 (2006).
14. Salinas, P.C. Modulation of the microtubule cytoskeleton: a role for a divergent canonical Wnt pathway. *Trends Cell Biol.* **17**, 333–342 (2007).
15. Anastasiadis, P.Z. *et al.* Inhibition of RhoA by p120 catenin. *Nat. Cell Biol.* **2**, 637–644 (2000).
16. Carothers, A.M. *et al.* Deficient E-cadherin adhesion in C57BL/6J-Min/+ mice is associated with increased tyrosine kinase activity and RhoA-dependent actomyosin contractility. *Exp. Cell Res.* **312**, 387–400 (2006).
17. Wennerberg, K. & Der, C.J. Rho-family GTPases: it's not only Rac and Rho (and I like it). *J. Cell Sci.* **117**, 1301–1312 (2004).
18. Krauthammer, M. *et al.* Exome sequencing identifies recurrent somatic *RAC1* mutations in melanoma. *Nat. Genet.* **44**, 1006–1014 (2012).
19. Kawazu, M. *et al.* Transforming mutations of *RAC* guanosine triphosphatases in human cancers. *Proc. Natl. Acad. Sci. USA* **110**, 3029–3034 (2013).
20. Mitchison, T.J. & Cramer, L.P. Actin-based cell motility and cell locomotion. *Cell* **84**, 371–379 (1996).
21. Lauffenburger, D.A. & Horwitz, A.F. Cell migration: a physically integrated molecular process. *Cell* **84**, 359–369 (1996).
22. Olson, M.F., Paterson, H.F. & Marshall, C.J. Signals from Ras and Rho GTPases interact to regulate expression of $p21^{Waf1/Cip1}$. *Nature* **394**, 295–299 (1998).
23. Karlsson, R., Pedersen, E.D., Wang, Z. & Brakebusch, C. Rho GTPase function in tumorigenesis. *Biochim. Biophys. Acta* **1796**, 91–98 (2009).
24. Gidekel Friedlander, S.Y. *et al.* Context-dependent transformation of adult pancreatic cells by oncogenic K-Ras. *Cancer Cell* **16**, 379–389 (2009).
25. Borrman, R. in *Handbuch der Speziellen Pathologische Anatomie und Histologie* 4th edn. (ed. Henke, F. & Lubarsch, O.) 812–1054 (Verlag von Julius Springer, Berlin, 1926).
26. Saito, A., Shimoda, T., Nakanishi, Y., Ochiai, A. & Toda, G. Histologic heterogeneity and mucin phenotypic expression in early gastric cancer. *Pathol. Int.* **51**, 165–171 (2001).
27. Henson, D.E., Dittus, C., Younes, M., Nguyen, H. & Albores-Saavedra, J. Differential trends in the intestinal and diffuse types of gastric carcinoma in the United States, 1973–2000: increase in the signet ring cell type. *Arch. Pathol. Lab. Med.* **128**, 765–770 (2004).
28. Hayashi, T. *et al.* The superiority of the seventh edition of the TNM classification depends on the overall survival of the patient cohort: comparative analysis of the sixth and seventh TNM editions in patients with gastric cancer from Japan and the United Kingdom. *Cancer* **119**, 1330–1337 (2013).
29. Kaneko, S. & Yoshimura, T. Time trend analysis of gastric cancer incidence in Japan by histological types, 1975–1989. *Br. J. Cancer* **84**, 400–405 (2001).
30. Shang, X. *et al.* Rational design of small molecule inhibitors targeting RhoA subfamily Rho GTPases. *Chem. Biol.* **19**, 699–710 (2012).
31. Shang, X. *et al.* Small-molecule inhibitors targeting G-protein-coupled Rho guanine nucleotide exchange factors. *Proc. Natl. Acad. Sci. USA* **110**, 3155–3160 (2013).

ONLINE METHODS

Informed consent and sample preparation. Frozen tissue samples of gastric cancer and paired normal gastric tissue samples were obtained from individuals who underwent gastrectomy at the University of Tokyo Hospital. Informed consent was obtained from all subjects, and this study was approved by institutional review boards at the University of Tokyo. We selected gastric tumor cases that pathologists histologically classified as DGC according to Lauren's classification. Depending on the size of the tissue sample, 15–60 sequential sections were cut at 20-μm thickness using a cryostat (Leica) at −20 °C. Total DNA was extracted from sections using the QIAamp DNA Mini kit (Qiagen).

Exome capture, library construction and sequencing. One microgram of DNA per sample was sheared with a Covaris SS Ultrasonicator. We used a Sciclone NGS workstation (Caliper Life Sciences) for automated library construction. Exome capture was performed with Agilent SureSelect Human All Exon Kit v4 (Agilent Technologies). Each sample was sequenced on an Illumina HiSeq 2000 instrument using a read length of 2 × 100 bp. Image analysis and base calling were performed using the Illumina pipeline with default settings. Summary statistics and data quality metrics for whole-exome sequencing are shown in **Supplementary Table 5**.

Exome sequence processing. Burrows-Wheeler Aligner (BWA)[32] and Novoalign software were used to align sequence reads to the human reference genome GRCh37/hg19. After removal of PCR duplicates, we used SRMA[33] to improve variant discovery through local realignments of short-read next-generation sequencing data. To identify somatic mutations in the low-tumor-content samples, we implemented an original variant caller and a method to estimate tumor cellularity as described below (karkinos genotyper; see URLs). For each sample, tumor cellularity was estimated from allelic imbalance in the matched tumor and normal samples with a program examining the allelic fractions of heterozygous SNPs in regions of loss of heterozygosity (LOH) using an algorism similar to that described in a previous report[34,35]. In some cases where LOH regions were not detected, tumor content ratios were estimated from the distribution of mutant allele frequencies. When both calculations failed to estimate tumor cellularity, we presumed it to be 0.2 for the correction of mutant allele frequencies. Consequently, somatic mutant allele frequencies, adjusted by estimated tumor content ratios, that were ≥15% were retained. Artifacts originating from errors in the sequence and mapping were also filtered out by checking SNV positions and base quality scores for supporting reads. Fisher's exact tests were then used, and SNV candidates with a P value of >0.2 were removed. To eliminate germline variations in this study, we carried out comparative analyses using paired tumor and non-tumor stomach mucosa tissues from the same cases for all of the samples analyzed and we extracted the somatic events detected only in tumor tissues. Annotation of SNVs was performed with ANNOVAR[36].

Gene selection for targeted resequencing. To accurately evaluate the frequency and distribution of somatic mutations, especially in stroma-rich DGCs, targeted resequencing was performed with deeper read coverage. To characterize *RHOA* gene and pathway aberrations, 27 genes were selected that included *RHOA*, RHO modulator genes (RhoGEF, RhoGAP and RhoGDI genes) and effector molecules (BioGRID and the Human Protein Reference Database (HPRD); see URLs). In addition, 19 genes were selected from recurrently mutated genes identified in previous gastric cancer exome studies[9,10] or in our discovery screen, including chromatin-remodeling, cell adhesion and WNT pathway genes. We selected 46 genes in total (listed in **Supplementary Table 2**).

Mutation confirmation using targeted resequencing. To validate somatic mutations in selected genes, we designed 2 panels consisting of 1,504 and 1,525 amplicons (average of 175 bp in length) for 46 genes in total (**Supplementary Table 2**) using DesignStudio for TruSeq Custom Amplicon (TSCA) sequencing (Illumina). Coverage was 98.9%, and 93.5% of the targeted regions were covered by the designed amplicons.

Library preparation for 87 DGC tumors and 51 IGC tumors with matched normal tissues was performed according to the TSCA protocol for Illumina paired-end sequencing. We performed 96-plex deep sequencing for each panel on one flow cell (two lanes) of a HiSeq 2500 instrument in rapid-run mode, using 150-bp paired-end reads. Low-quality parts of the reads, 5 bp from both ends of raw reads, were trimmed off, and the remaining sequences were mapped to the reference hg19 genome using BWA. Initial detection of SNVs and indels was carried out using the Genome Analysis Toolkit (GATK) UnifiedGenotyper with a minimal coverage of 20-fold. Any variants detected in pooled normal data were filtered out as possible germline variants, such as SNPs or errors in PCR amplification and sequencing. Finally, we inspected the mapped reads and called mutations on the Integrative Genomics Viewer (IGV) to confirm the variations. We could not obtain any sequence reads from a part of exon 2 of *RHOA* in several samples, possibly owing to primer synthesis failure; therefore, we performed PCR amplicon sequencing targeting exon 2 of *RHOA* using the Nextera XT DNA sample prep kit (Illumina) according to the manufacturer's protocol and generated 200-bp paired-end reads on a MiSeq system (Illumina). Summary statistics and data quality metrics for TSCA sequencing are shown in **Supplementary Table 5**.

Digital PCR. Digital PCR was carried out using the BioMark nanofluidics system (Fluidigm) with the 12.765 Digital Array. Assay methods were essentially as described[37]. Briefly, reaction mixture was prepared for each assay, containing 1× TaqMan gene expression master mix, 1× *RHOA*wt-FAM and *RHOA*mut-VIC TaqMan assay probes, 1× sample loading reagent (Fluidigm) and 2 μg of genomic DNA. The *RHOA* DNA fragment was amplified, and, at the end of each PCR cycle, FAM and VIC signals for all chambers were recorded. For each panel, both FAM-positive chambers (wild type) and VIC-positive chambers (mutant) were counted, and the mutant/wild-type copy number ratio was calculated as described[38]. Primer sequences are shown in **Supplementary Table 6**.

Immunohistochemistry for HER2 protein. Paraffin-embedded blocks of gastric tumors were cut into 4-μm sections just before immunohistochemical analyses of HER2 protein. Immunohistochemical staining was performed using the Ventana Benchmark XT autostainer (Ventana Medical Systems) with the labeled streptavidin-biotin peroxidase method, and signals were visualized with 3,3′-diaminobenzidine. The primary antibody used was an antibody to HER2 (4B5, Ventana Medical Systems). Antigen epitopes were retrieved by heating at 100 °C for 60 min with EDTA, pH 8.5 (Ventana Benchmark CC1 standard program). The method by which HER2 immunostaining was scored was based on a previous report[36].

Microscope-based dissection. Sections (10 μm) were sliced from paraffin blocks and mounted on glass slides. Another 4-μm section was sliced for staining with hematoxylin and eosin. After areas with intramucosal tubular components and poorly differentiated cohesive components were examined by microscope, these components were dissected from the corresponding 10-μm sections.

Cell culture. The human SW948, BT474, AGS (obtained from the American Type Culture Collection, ATCC), OE19 (obtained from the European Collection of Cell Cultures, ECACC) and MKN74 (obtained from the Japanese Collection of Research Bioresources, JCRB) cancer cell lines were cultured in Leibovitz's L-15 (Gibco), Hybri-Care Medium (American Type Culture Collection), RPMI-1640 (Sigma), F12K (Gibco) and RPMI-1640 (Sigma), respectively, supplemented with 10% FBS (PAA Laboratories) at 37 °C with 5% CO_2, except for SW948 cells, which were cultured without CO_2. Cells were passaged once every 2–3 d.

siRNA transfection, cell growth inhibition assays and gain-of-function rescue assays. siRNA duplex oligonucleotides against human *RHOA* (*RHOA* siRNAs 2 and 3) and *KIF11* and a non-targeting negative control siRNA (Silencer Select Negative Control No.1 siRNA) were synthesized by Life Technologies (**Supplementary Table 6**). Cells were seeded in 96-well ultra-low-attachment plates (Corning) at a density of 1.0×10^4 cells per well in triplicate wells. At the same time, mixtures of siRNA and Lipofectamine RNAiMAX reagent (Invitrogen) were added to each well as 0.2 or 1 nM siRNA solutions. Under these culture conditions, SW948, BT474, OE19, AGS and MKN74 cells showed spheroid-like growth patterns. ATP molecules were